Master WAVES

Waves, Acoustics, Vibrations, Engineering and Sound

ACOUSTIC CHARACTERIZATION OF POROUS MATERIALS USING A PU PROBE

Master Thesis

Author: Marco Antonio Ribera Tejeda

Tutors: Rui Ribeiro (Amplitude Acoustics)

Paulo Amado Mendes (UC)

Coimbra, Portugal. September 2023

Acknowledgments

This has undoubtedly been an extraordinary journey, for which a special space for showing my gratitude is needed. This work represents the culmination of my master's degree, but more importantly, the culmination of a dream. A dream that has become a reality thanks to the contributions of different people, which I would like to acknowledge in this space.

To my parents, who have supported me on every step of the journey. I wouldn't be here without your unconditional love, which has given me strength even in the most difficult moments of this journey. Also, my sister and Lu, whose love I carry wherever I go.

To my supervisors, Paulo Amado Mendes and Rui Ribeiro, for your guidance and support along the project. I feel grateful for all the lessons and all the knowledge that you have shared with me. Also, to Pedro Pinto, for your guidance through the experimental procedures that took place in Amplitude Acoustics. From DEC, I would also like to mention Prof. Luis Godinho and my colleagues Laura Sousa and Denilson Ramos, whose support and guidance helped me immensely throughout this internship.

To my beautiful friends, who, even when separated in distance, have always remained close to me. All my colleagues from the Master WAVES, who have turned into close friends, I couldn't imagine this journey without you. It has been an incredible experience along your side.

Finally, to the WAVES Coordinators, Paulo Amado Mendes, Bruno Lombard, and Javier Redondo, for believing in me and taking me into the Master WAVES' first cohort. I acknowledge all the effort you have put into building this program. It has been a great growing and learning experience, which would not have been possible without you.

Abstract

The PU probe technique allows in-situ surface impedance measurements of porous materials with minimal sample preparation and measurement setup. However, this technique comes at the cost of multiple additional factors, which can influence the results if not carefully addressed. In this work, a sensitivity analysis is performed for two different materials, Rockwool and Melamine foam, aiming to provide a set of guidelines on how to perform measurements with the PU probe technique regarding sample size, sound field model and probe location. Below 800 Hz, the influence of these factors proved to be significant. Nonetheless, results showed to be accurate at higher frequencies, yielding errors smaller than those obtained by the impedance tube, in reference to the Johnson-Champoux-Allard (JCA) and the Delany-Bazley-Miki (DBM) equivalent fluid models.

The PU Probe technique was then compared with the current standardized procedures by converting all measured normal incidence sound absorption data into random incidence absorption coefficients of infinite lateral dimensions. This was achieved by a model fitting procedure applied to both Impedance Tube and PU Probe normal incidence measurements. The model fitting procedure enabled the inverse estimation of the main non-acoustical macroscopic parameters of the materials employing the JCA and the DBM models, finding good agreement with the macroscopic parameters determined through direct methodologies. Furthermore, this procedure enabled obtaining broadband normal and diffuse field sound absorption coefficients from the PU Probe measurements. Excellent agreement was found between all measured and reference curves for both materials at normal incidence. In a diffuse field, despite the non-diffuseness found in the measurement chamber, the measured absorption after a size correction was found to be oscillating around the reference curve, from which good agreement between the Impedance Tube and the PU Probe techniques was found.

INDEX

1 INTRODUCTION

Sound-absorbing materials play a crucial role in various applications, ranging from noise control to architectural acoustics, enabling us to enhance the sonic environment and improve our quality of life. The growing trends of urbanization and industrial development have made effective noise mitigation strategies a necessity as the environments where we live and work become increasingly noisier. The use of porous materials constitutes a common and versatile solution, capable of efficiently absorbing sound energy across a wide frequency range. Current efforts are being focused on the development of sustainable and cost-efficient materials while providing good acoustic features [1].

As computational models continue to advance, acousticians and designers can now perform simulations to evaluate noise control and room acoustic solutions. However, the accuracy of these models heavily relies on the input data they are provided with. Consequently, the proper measurement and characterization of sound-absorbing materials is crucial for achieving reliable acoustic simulations. Relying solely on databases or manufacturer-provided data, which often needs more specific frequency details and is presented in octave bands, may not suffice for accurate modeling.

Traditional reverberant chamber methods often demand large sample areas, which may not be feasible for the development of new materials, particularly considering economic constraints. In contrast, using an impedance tube for measurements could offer a more viable solution. However, this approach comes with its own set of limitations, such as the normal incidence restriction and the additional sample preparation and manipulation required. Free-field methods, developed in recent years, could become a solution to address these limitations [2].

This work was developed at the Institute for Sustainability and Innovation in Structural Engineering (ISISE), located within the Department of Civil Engineering at the University of Coimbra. Most of the research and experimental procedures were conducted within this institution. Additionally, valuable collaborations were established with Amplitude Acoustics, an acoustic consulting firm and industrial partner of the Master WAVES, which played a pivotal role by hosting and providing essential resources for the collection of in-situ experimental data.

1.1 MOTIVATION

The existing standardized techniques employed for the acoustic characterization of materials reveal discernible limitations. Despite promising outcomes achieved through advancements in free field methods, their application for in-situ measurements presents challenges, as the unique conditions of such measurements introduce additional uncertainties that can lead to inaccuracies. Moreover, comprehending these techniques through available research is complicated, given the scarcity of literature and the diversity of approaches adopted by various authors.

Enhancing the understanding of free field methods applied under in-situ conditions and the pertinent influencing variables holds substantial importance for both the scientific and industrial sectors. Within the realm of acoustic consultancy firms, the quest for precision in parameters is paramount to fulfill the client requirements. By delving deeper into the intricacies of this technique and scrutinizing its surrounding complexities, we can significantly contribute to advancing acoustic characterization methodologies, thereby yielding benefits for both research endeavors and practical applications.

1.2 OBJECTIVES

To fulfill the purpose of this study, the proposed objectives to be achieved through this dissertation are the following:

- Model absorbent porous materials through the “Equivalent Fluid Theory”;
- Perform a sensitivity analysis, comparing different calculation methods, sample size and PU Probe locations;
- Suggest a solution to the limitations of the PU Probe measurement technique;
- Propose a method to compare the results from the PU Probe to the standardized methods;
- Provide a guideline that can easily be retrieved to perform measurements with the PU Probe.

1.3 THESIS STRUCTURE

This thesis begins by introducing the topic of in-situ acoustic characterization of materials, including the motivations behind this research and the specific objectives aimed to be achieved.

Chapter 2 serves as the foundation of this work, offering an overview of the fundamental concepts related to wave propagation and porous materials.

Chapter 3 comprises a comprehensive literature review, exploring concepts associated with the acoustic characterization of porous materials along with past investigations carried out in this domain.

In Chapter 4, the methodologies employed to accomplish the set objectives are detailed. This includes the procedures followed for the standardized methods, the sensitivity analysis for the PU Probe, the model fitting procedure, and the considerations made for comparing the different techniques.

Moving on to Chapter 5, the results obtained from all experimental methods and the model fitting procedure are presented, along with their thorough discussion and interpretation.

Chapter 6 concludes the thesis by summarizing the key findings of this study and providing suggestions for future research directions.

2 GENERAL CONCEPTS

2.1 WAVE PROPAGATION

A sound wave is created by a disturbance in a medium, such as air, that causes particles of the medium to vibrate. This phenomenon generates temporal and spatial changes in a fluid density, which can be translated into pressure and particle velocity variations. A plane wave equation can be obtained from the relation of the equation of state for linear acoustic waves, simplifying for small changes in density and pressure

$$\nabla^2 p(\vec{r}, t) - \frac{1}{c^2}\frac{\partial^2 p(\vec{r}, t)}{\partial t^2} = 0 \tag{2.1}$$

where $p(\vec{r}, t)$ is the pressure with position vector $\vec{r}$ and time variable t, c is the speed of sound in air given by $c^2 = \frac{\rho_0}{\gamma P_0}$, where ρ_0 being the medium's density, γ is the ratio of specific heats and P_0 the atmospheric pressure, and $\nabla^2 = \partial^2/\partial x^2 + \partial^2/\partial y^2 + \partial^2/\partial z^2$ is the Laplacian scalar operator. The sound field can be represented in a simple form considering plane wave propagation, indicating that both pressure and velocity are uniform over the direction of propagation. By a complex exponential representation to indicate the harmonic time dependence, the plane pressure field with complex amplitude $\tilde{p}$ is represented as

$$p(x,t) = \tilde{p}(x)e^{i\omega t} \tag{2.2}$$

with $i = \sqrt{-1}$. This enables to solve equation (2.1), becoming the Helmholtz equation, which in one dimension takes the form of a linear, second-order ordinary differential equation

$$\frac{d^2\tilde{p}(x)}{dx^2} + k^2\tilde{p}(x) = 0 \tag{2.3}$$

where $k = \frac{\omega}{c}$ is the wavenumber, $\omega = 2\pi f$ the angular frequency. Particle velocity carries information regarding the wave propagation direction, and it is related to the acoustic pressure by Euler's equation, given by

$$\rho_0 \frac{\partial u(\vec{r},t)}{\partial t} = -\vec{\nabla} \cdot p(\vec{r},t) \tag{2.4}$$

where $\vec{\nabla} \cdot p(\vec{r},t)$ is the gradient of pressure. When describing traveling harmonic plane waves, the particle velocity propagating along the x direction is obtained as the ratio of acoustic pressure to the characteristic impedance of the medium Z_0 [3]. For a spherical representation of the sound field, the Laplacian in equation (2.1) can be substituted by a Laplacian in a spherical coordinate system, becoming a function of time and the radial coordinate r [4]

$$\frac{\partial^2 p}{\partial r^2} + \frac{2}{r}\left(\frac{\partial p}{\partial r}\right) = \frac{1}{c^2}\frac{\partial^2 p}{\partial t^2}. \tag{2.5}$$

General solutions for acoustic pressure and particle velocity can thus be obtained for a symmetric sound field

$$p(x,t) = \frac{\tilde{p}}{r}(x)e^{i\omega t} \tag{2.6}$$

$$\frac{\tilde{p}}{\tilde{u}} = \rho_0 c \frac{ikr}{ikr+1} \tag{2.7}$$

The time factor $e^{i\omega t}$ will be used throughout this work.

2.2 POROUS MATERIALS

Porous materials consist of two phases: a fluid phase and a solid phase, and the dissipation of energy occurs through their interaction. The primary sources of energy losses in porous materials stem from viscous boundary layer effects, caused by friction between the fluid near the solid boundaries, and thermal losses resulting from heat transfer between the fluid and solid phases. While vibration-induced losses can also be present, they typically have a lesser impact [5].

A diverse range of materials exhibits porous characteristics, including foams, soil, mineral wools, carpets, activated carbon and aerosols. Recent research in the field of porous materials has seen a significant emphasis on the development of sustainable and environmentally friendly porous absorbers. There is a growing interest in utilizing recycled materials and exploring renewable sources to mitigate the environmental impact associated with traditional porous materials [1]. By focusing on novel and sustainable alternatives, researchers aim to create porous materials that not only offer excellent energy dissipation properties but also contribute positively to environmental conservation and resource management.

These materials can be further categorized based on their structural properties, with the majority falling into three main categories: fibrous materials, foam absorbers and granular absorbers. However, the intricate and complex microscopic structure of each type of absorber presents challenges in accurately describing their acoustic behavior using detailed internal characteristics. As a result, models primarily rely on macroscopic material properties to effectively characterize their sound absorption capabilities.

2.2.1 Non-Acoustic Properties

Non-acoustical properties are needed to predict sound propagation and modeling of porous materials. The flow resistivity (σ) is the most important parameter for the characterization of porous materials. It quantifies the degree to which air can permeate a porous material and the level of opposition encountered by airflow when passing through the material's structure, normalized by the sample thickness. It can be obtained analytically by

$$\sigma = \frac{\mathrm{AR}}{\mathrm{d}}, \tag{2.8}$$

where $\mathrm{d}[\mathrm{m}]$ is the thickness of the specimen in the direction of flow, $\mathrm{A}[\mathrm{m}^2]$ is the cross-sectional area perpendicular to the direction of flow and R is the flow resistance, given by:

$$R = \frac{\Delta p}{q_V} = \sigma d\,, \tag{2.9}$$

where $\Delta p\ [\mathrm{Pa} = \mathrm{N/m^2}]$ is the air pressure drop across the test specimen with respect to the atmosphere and q_V is the volumetric airflow rate, in cubic meters per second, passing through the test specimen. The flow resistivity unit is Ns/m^4 or $rayls/m$. This parameter exhibits the greatest variability among porous materials, making its determination crucial.

ISO 9053 [6] describes two methods for measuring the volumetric airflow rate and pressure drop between two faces of a specimen: the direct airflow method and the alternating airflow method. These methods differ depending on the airflow source, which is either produced by a pressure depression system or a piston. Alternative or indirect methods, such as with impedance tubes [7], coupled cavities [8], or inverse methods based on optimization procedures, which have yielded good results and can provide a reasonable estimation of the flow resistance and resistivity, when the special apparatus of the standard is not available [5].

The flow resistivity is the main input for empirical models, such as Delaney-Bazley [9] and their modifications by Miki [10]. However, this simplified approach does not consider other significant properties of porous absorbers, for which more detailed models can predict sound propagation with additional properties such as porosity, tortuosity, and viscous and thermal characteristic lengths.

The Porosity or Open Porosity is given by the ratio of total open pores volume V_{op} to the total volume of the material V_t,

$$\phi = \frac{V_{op}}{V_t}\,. \tag{2.10}$$

Several techniques have been proposed to measure this ratio, varying on the type of porous solid to be tested. For instance, the pore volume can be calculated by measuring the mass of the sample when saturated by a liquid and by air, by the Archimedes principle or law of buoyancy. Another simple technique based on the same principle consists of measuring the mass in air and vacuum [11]. Porous materials, including fibrous and cellular materials, typically have a relatively small solid phase volume, resulting in a porosity value that is typically very high, close to unity.

The alignment of pores in relation to the incoming sound field influences sound propagation. This impact is captured by the parameter Tortuosity, represented as α_∞. The tortuosity level in the material determines how convoluted the sound propagation path becomes. In the high-frequency

range, tortuosity serves as a geometric parameter that characterizes the sinuous pore network and the coupling between the fluid and the structure of the material. Several methods for tortuosity measurement exist, including ultrasound techniques, by measuring the time of arrival of the signal with and without a sample between the emitter and receiver, calculated by

$$\alpha_\infty = \lim_{\omega \to \infty} \left(\frac{c_0}{c(\omega)} \right)^2 \tag{2.11}$$

with c_0 being the sound speed and $c(\omega)$ the wave speed in the material. The tortuosity value for porous materials is typically near the lowest possible value, being $\alpha_\infty = 1$. However, as the propagation path becomes more complex or the pore angle with respect to the surface increases, the tortuosity tends to rise above unity.

The pore's geometry can also play a significant role in sound absorption due to its influence on the surface area, leading to alterations in the thermal and viscous behavior [5]. The viscous characteristic length Λ [m] represents the impact of viscous effects in the mid to high-frequency range and is an indicator of the size of narrow pores. Furthermore, in the analysis of heat conduction at high frequencies, the thermal characteristic length Λ' [m] is an indicator of the size of large pores, where heat exchange is privileged. This corresponds to the surface-to-volume ratio of unweighted pores. A relation between the viscous characteristic length with the non-acoustical parameters described in the above section, is given by [5]

$$\Lambda = \frac{1}{s} \sqrt{\frac{8\eta\alpha_\infty}{\phi\sigma}}, \tag{2.12}$$

where s is the cross-sectional shape factors of the pore and η is the dynamic viscosity of air, which at $20^{o}\mathrm{C}$ is $1.82 \times 10^{-5}\ [Pa \cdot s]$. Approximations can be done by considering specific pore geometries, such as considering the shape factor as 1 by considering circular pores, and $\Lambda = \Lambda'$ for rigid framed fibrous materials [12]. Values range in the order of micrometers, and the thermal characteristic length is usually greater than its viscous counterpart. Based on ultrasonic transmission measurements, both characteristic lengths and tortuosity can be simultaneously deduced when the material is saturated by two different gases, such as helium or argon [13]. In practice, since the pores in porous materials are not formed by a singular geometry, the characteristic lengths are commonly found inversely through model-fitting procedures.

2.2.2 Acoustic Properties of Materials

A material surface can be characterized by four acoustic properties: surface impedance, admittance, reflection coefficient and absorption coefficient. These quantities provide valuable information about the nature of the surface and how it interacts with sound waves. Surface impedance and admittance are related to the magnitude of the reflected sound wave and the phase shift induced by the surface on the wave. The reflection coefficient, on the other hand, describes the ratio between the reflected wave and the incident wave. It is used to evaluate the energy transfer between the two waves. Finally, the absorption coefficient is a ratio of the absorbed and incident energy, and it is often used to evaluate the acoustic performance of materials in various applications.

2.2.2.1 Characteristic Impedance

The characteristic impedance Z_{ca}, referred to in the literature as specific, acoustic, or a combination, can thus be obtained as the ratio of the complex amplitude of the sound pressure to the specified vector component of the particle velocity.

$$Z_{ca} = \frac{p(x,t)}{u_x(x,t)} = \rho c = \sqrt{\tilde{\rho}_e \tilde{K}_e} \tag{2.13}$$

The characteristic impedance of a medium is a very useful property, which denotes the resistance of the medium to pressure excitation, or the pressure required to induce movement in the medium's particles. It can also be characterized in terms of the effective density, $\tilde{\rho}_e$, and Bulk Modulus, $\tilde{K}_e$, by means of the Newton-Laplace formula $\tilde{K}_e = \rho_e c^2$, referring to the density experienced by the sound waves.

For air, the characteristic impedance $Z_0 = \rho_0 c_0$ is purely real. Considering the density and sound speed in air, commonly taken as $\rho_0 = 1.213\ [kgm^{-3}]$ and $c_0 = 20\sqrt{273 + T} \approx 343\ [ms^{-1}]$, at $T = 20°C$, it has a value of about $415[kg/m^2s]$. In porous media, this value becomes complex. Along with the characteristic impedance, the propagation wavenumber becomes complex in a porous medium, and can also be obtained in terms of the effective density and bulk modulus of the medium

$$k = \frac{\omega}{c} = \omega\sqrt{\frac{\tilde{\rho}_e}{\tilde{K}_e}}\ . \tag{2.14}$$

To evaluate the sound energy absorbed, reflected and transmitted, the surface impedance, or the specific impedance at the boundary between two different media is needed,

$$Z_s = \frac{p(B_2)}{u(B_2)}, \tag{2.15}$$

where B_2 is a point at the boundary of two fluids. Due to pressure and velocity continuity at the boundary, the impedance at both points at the interface, B_2 and B_3, is equal.

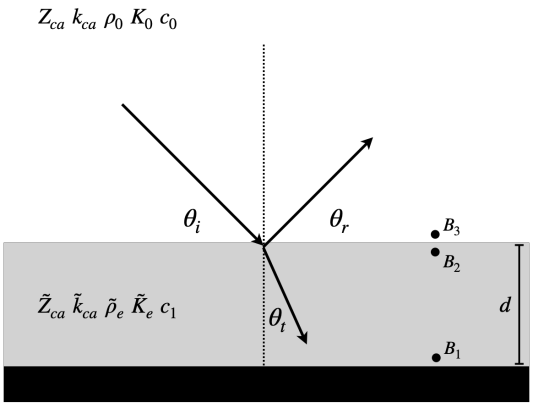

Figure 2.1: Oblique incidence plane wave over an infinite absorber

By the assumption of plane wave propagation, the surface impedance can be obtained from the characteristic impedance and wavenumber of the fluid by the Transfer Matrix Method (TMM)

$$Z_s = \tilde{Z}_{ca} \frac{-iZ(B_1)\mathrm{cotg}(\tilde{k}_{ca}d) + \tilde{Z}_{ca}}{Z(B_1) - iZ_{ca}\mathrm{cotg}(\tilde{k}_{ca}d)}, \tag{2.16}$$

where $Z(B_1)$ is the surface impedance of the backing material and d is the thickness of the sample. In the case of a single layer, rigidly-backed as shown in Figure 2.1, $Z(B_1) = \infty$ thus simplifying to

$$Z_s = -i\frac{\tilde{Z}_{ca}}{cos(\theta_t)}\cot(\tilde{k}_{ca}\cos(\theta_t)d). \tag{2.17}$$

The relation between the incident and transmitted angles is obtained from the Snell-Descartes law,

$$\theta_t = \arcsin\left[\left(\frac{k_0}{\tilde{k}_{ca}}\right)\sin(\theta_i)\right]. \tag{2.18}$$

The surface impedance is often normalized with respect to the characteristic impedance of air. The normalized surface impedance is a complex quantity in which the real and imaginary parts are denoted by the characteristic surface resistance (r_n) and reactance (x_n) ratios [4], respectively, as $\zeta = r_n + ix_n$. Both terms influence the absorption coefficient, the resistance being associated with energy losses, and the reactance to phase changes [5].

The admittance is simply the reciprocal of the impedance. As the impedance, the surface admittance is normalized to the characteristic impedance of air,

$$\beta = \frac{1}{Z_s}. \tag{2.19}$$

2.2.2.2 Reflection and Absorption coefficients

The pressure reflection coefficient or reflector factor is the ratio between the reflected and incident energies at the surface of a layer, which can be given, in terms of pressure or intensity by

$$R = \frac{P_R}{P_I}. \tag{2.20}$$

For plane waves with angle of incidence θ_i, the relation between the surface impedance and the reflection factor is given by

$$R(\theta_i) = \frac{Z_s \cos\theta_i - Z_0}{Z_s \cos\theta_i + Z_0} \tag{2.21}$$

The absorption coefficient is then defined as the ratio between the absorbed and the incident energy flux, which can be deduced from the complex reflection coefficient as

$$\alpha = 1 - |R(\theta_i)|^2. \tag{2.22}$$

3 STATE-OF-THE-ART

This chapter presents a literature review, delving into the essential concepts related to the acoustic characterization of sound-absorbing porous materials. A comprehensive overview of prior research conducted in this field is provided. Notably, this chapter offers a detailed exposition of the PU Probe technique.

3.1 MAIN MEASUREMENT TECHNIQUES

In this subchapter, the main techniques regarding the measurement of the absorption coefficient are presented, along with their limitations. Free-field techniques are further introduced.

3.1.1 Reverberant Chamber

Three main methods are available to measure the acoustic parameters of materials, but only two have been thoroughly developed and standardized. The Reverberant chamber allows deducing a diffuse field absorption coefficient of a sample by the effect of the rate of decay of sound in a room, with and without the sample, assuming a perfectly diffuse field. It is thus commonly referred to as “Sabine’s Absorption Coefficient.” The international Standard ISO 354:2003 [14] specifies the measurement methodology, relying on Sabine’s equation to obtain the equivalent absorption area of the sample.

In practice, it is difficult to achieve a perfectly diffuse field, especially below the Schroeder frequency, where the modal behavior of the room dominates. ISO 354 presents a method to determine the optimum number of diffusers to achieve an adequate diffuse field for measurements. However, different rooms with different shapes and volumes may result in high levels of uncertainty as well as large discrepancies in the absorption coefficients compared to the theoretical random incidence sound absorption coefficient [15].

Furthermore, apart from non-diffuseness, another important issue when extrapolating the measured absorption coefficient in the reverberant chamber method into real rooms are the edge effects, which results in an increased absorption when measuring with this technique due to the diffraction effects from the samples' edges [16]. Determining of the absorption of the edges or extrapolating to the wished sample sizes might be a solution, which might be crucial for accurate absorption characterization.

The measurement chamber must have a volume of at least $200m^3$. Additionally, large sample areas are required, varying between 10 and $12m^2$, depending on the volume of the reverberant chamber, which often may not be feasible during the research and development of new materials. The high cost of these conditions often limits their application, leading to the use of Impedance Tube measurements instead.

3.1.2 Impedance Tube

The impedance tube technique, also known as the Kundt tube, is widely used because only small samples are needed. Several parameters can be retrieved in a short amount of time, using, for example, the transfer-function method standardized by ISO 10534-2 [17]. Unlike the reverberant chamber technique, only plane waves at a normal incidence angle are considered. Therefore, the resulting absorption coefficient is addressed as the normal incidence absorption coefficient and cannot be directly compared with the one measured in the reverberant chamber.

Despite its advantages, this method requires careful sample preparation and manipulation at multiple sample diameters, which may be challenging for certain materials, such as lower-density porous materials. Moreover, differences between the sample and the actual implementation of the material may result in differences in acoustic properties.

Impedance tubes can be adapted for in-situ measurements. Portable impedance meter system for measuring the impedance of acoustic liners in their final condition have been developed, with a focus on aerospace applications [18]. However, the sealing method is critical. Leakage or material deformation can lead to erroneous measurements. Therefore, this method may be useful for stiff or rigid materials where good sealing can be achieved, such as road surfaces, for which an standardized method has been stablished [19]. For softer, porous materials, free-field techniques might be preferred.

3.1.3 Free Field Methods

The free field techniques originated from a generalization of the Impedance Tube technique, with the aim of measuring the acoustic impedance of ground surface [20]. Different approaches have been taken, using either pressure sensors (PP), particle velocity (UU), or a combination of both (PU). The PP-method, which similarly to the Kundt Tube requires the measurement of pressure using two microphones and the obtention of a transfer function. The UU-method, similarly to the PP relies on obtaining the impedance from a transfer function of two particle velocity sensors at two locations.

The PU method, which requires the measurement of acoustic pressure and particle velocity, measures the specific impedance near the surface of the sample. In a study comparing the three above-mentioned methods, the sample size was proved to have a major impact on the

measurements, producing higher errors when testing smaller samples. The PU method was found to be the most stable against sample size, as well as to source height [2].

The integration of the PU Probe into a handheld setup, often termed an "Impedance gun," has facilitated research with this device. Nevertheless, numerous factors add complexity to measurements employing this device. Valid results from this setup are expected in a frequency range from 300Hz-10000Hz. The lower boundary of this range is primarily limited by the models needed for extracting the surface impedance and signal-to-noise ratio issues encountered at the pressure and particle velocity sensors [21].

3.2 SIMULATION WITH EQUIVALENT FLUID MODELS

To model sound propagation in porous media and thus calculate the relevant absorption coefficient, these materials can be modeled as equivalent fluid materials, where only the airborne wave propagates in the pores of the material. Several models have been developed through empirical and analytical approaches.

3.2.1 Delany-Bazley-Miki model

The Delany-Bazley-Miki (DBM) is a well-known equivalent fluid empirical model, based on regression models and large number of Impedance Tube measurements on porous materials [9, 10]. Assuming porosity and tortuosity near unity, this model can estimate the characteristic impedance and complex wavenumber from the flow resistivity, respectively, by

$$\tilde{Z}_{ca} = \rho_0 c_0 \left[1 + 5.50\left(10^3 \frac{f}{\sigma}\right)^{-0.632} - j8.43\left(10^3 \frac{f}{\sigma}\right)^{-0.632}\right] \tag{3.1}$$

$$\tilde{k}_{ca} = \frac{2\pi f}{c_0}\left[1 + 7.81\left(10^3 \frac{f}{\sigma}\right)^{-0.618} - j11.41\left(10^3 \frac{f}{\sigma}\right)^{-0.618}\right]. \tag{3.2}$$

3.2.2 Johnson-Champoux-Allard model

The Johnson-Champoux-Allard (JCA) is a more complex semi-analytical phenomenological model requiring the flow resistivity, open porosity, tortuosity, and viscous and thermal characteristic lengths to describe the visco-inertial and thermal effects, through the effective density and Bulk modulus [3]

$$\tilde{\rho}_e = \frac{\alpha_\infty \rho_0}{\phi}\left[1 + \frac{\sigma\phi}{j\omega\rho_0\alpha_\infty}\sqrt{1 + \frac{4i\alpha_\infty^2\eta\rho_0\omega}{\sigma^2\Lambda^2\phi^2}}\right] \tag{3.3}$$

$$\widetilde{K}_e = \frac{\gamma P_0}{\phi}\left(\gamma - (\gamma-1)\left(1 + \frac{8\eta}{i\Lambda'^2 N_p\omega\rho_0}\sqrt{1 + \frac{i\Lambda'^2 N_p\omega\rho_0}{16\eta}}\right)^{-1}\right)^{-1}. \tag{3.4}$$

Characteristic complex impedance and wavenumber can be then obtained from the effective density and Bulk modulus by means of equations (2.13) and (2.14), respectively. These models, however, do not take into account elastic frame resonances nor structure-fluid interaction, which can be accounted, for instance, by the Biot model. The former, however, requires additional parameters further complicating its applicability. Nonetheless, good agreement between these models has been found [22], enabling them to be used as reference models for a vast majority of porous materials.

3.3 IMPEDANCE MEASUREMENTS WITH A PU PROBE

The Pressure-Velocity probe, or PU Probe, is a sensor that integrates a free-field omnidirectional microphone and particle velocity sensor closely positioned next to each other. The velocity sensor consists of two wires that detect the heat transfer induced by an incoming acoustic wave. This creates a differential electrical resistance, which is measured and enables quantifying the particle velocity. Within an Impedance Gun measurement system, it comprises a loudspeaker in a spherical housing mounted on a decoupled metallic structure to a PU probe at a fixed distance $r = 26\mathrm{cm}$.

Performing in-situ measurements using a portable system offers several advantages, including non-destructive assessments directly on the final application form of the material, without the need for sample preparation or dedicated laboratory space. However, it's important to consider various additional factors that come into play during in-situ measurements, such as the measurement environment and the probe calibration. Furthermore, the compact design of the device necessitates making certain compromises due to the short source-to-probe distance, and due to the sound field model requirement to derive the surface impedance from the measured specific acoustic impedance. To ensure accurate and reliable measurements using this technique, a comprehensive understanding of these factors and their implications is essential.

3.3.1 Probe location

Numerically and under the free-field assumption, measuring with the probe at the center of the sample has yielded higher errors than off-center when the sound source position was set fixed in the center of the sample [23]. By means of a Boundary Element Method (BEM) model, a measurement region that minimizes this error was determined empirically in that work. The so-called "confidence region" is dependent on the sample size only, which for square samples takes the form of a circle centered with radius $a \approx 0.3L$, where L is the length of the rectangle. It is thus interesting to compare experimentally and under in-situ conditions the receiver position both at center and off-center positions. The probe-to-sample distance has been studied in depth for different porous materials [21, 24, 25]. Their findings consistently indicate that positioning the probe as close as possible to the specimen yields optimal results, regardless of the calculation method employed.

3.3.2 PU Probe Calibration

For impedance measurements, a free-field impedance calibration technique is commonly preferred, which consists of obtaining a transfer function of the theoretical impedance considering the source as a monopole Z_0, calculated by equation (2.7), and the impedance measured under approximated free-field conditions Z_{ff}. A calibration factor is then obtained by

$$\mathrm{CF} = \frac{\mathrm{Z}_0}{\mathrm{Z}_{\mathrm{ff}}}\,. \tag{3.5}$$

This calibration factor is then applied to the measurements taken above the sample, taking into consideration the in-situ atmospheric conditions inherent to the measurement environment.

$$\mathrm{Z}_{\mathrm{m}} = \left(\frac{\mathrm{p}_{\mathrm{m}}}{\mathrm{u}_{\mathrm{m}}}\right) \cdot \mathrm{CF}\,. \tag{3.6}$$

Applying this calibration technique enables correcting all subsequent impedance measurements with a maximum error within +-0.3dB in amplitude and +-2 degrees in phase for the source to probe distance used, within the frequency range of the system used (300Hz-10 kHz) [21]. Although simple, contributions from parasitic reflections as well as background noise can affect the correction function at low frequencies whenever measuring under non-anechoic conditions, at which time windowing techniques are not effective [26]. Impedance tube calibration techniques can achieve better results at lower frequencies. However, its validity range is limited, bounded by the tube dimensions [27].

3.3.3 Measurement environment

Until now, most of the research has been centered on measurements within anechoic or semi-anechoic settings. However, recent investigations have extended to explore the influence of ambient noise and reflections, carrying out experiments in diverse reverberant surroundings [25, 28]. Results from these studies show that a meticulous choice of a sound field description model is a significant consideration for in-situ measurements, as certain proposed sound field models exhibit a higher sensitivity to the environment factor [25].

3.3.4 Sound field description models

The characteristic surface impedance of the sample can be extracted from the measured impedance at the probe location by means of a description model of the pressure field. The PU probe positioned close to the surface of the sample measures the incident and reflected field, which is captured into a specific acoustic impedance Z_m at the measurement location. In the simplest case, by the assumption of plane incident waves, the specific acoustic impedance is obtained as

$$Z_m = \frac{p_{tot}}{u_{n,tot}} = \frac{p_{inc} + Rp_{inc}}{\frac{\cos(\theta)}{\rho_0 c_0}(p_{inc} + Rp_{inc})} \tag{3.7}$$

where p_{inc} is the incident pressure, and θ the incidence angle. This assumption enables the direct calculation of the planar reflection coefficient R by means of equation (2.21). The surface impedance Z_s from Z_m can be estimated as [29]

$$Z_s = \frac{Z_m + i\tan(k_0 h)}{1 + i\,Z_m \tan(k_0 h)}, \tag{3.8}$$

where h is the distance between the probe and the surface of the sample. The plane incidence wave assumption in the free field cannot be held true at low frequencies or when the source is close to the probe due to the sphericity of the incoming waves [30], being this method only a good approximation when $kr >> 1$ [21]. In practice, physically addressing these limitations would downgrade the portability of an in-situ measurement system, for which more complex sound field methods that approximate spherical wave propagation can represent a better solution. The Mirror Source Model is a more robust yet simple method, describing the sound field above the sample

due to a point source (Figure 3.1). The impedance from a spherical source is approximated as the impedance from a monopole given by equation (2.7).

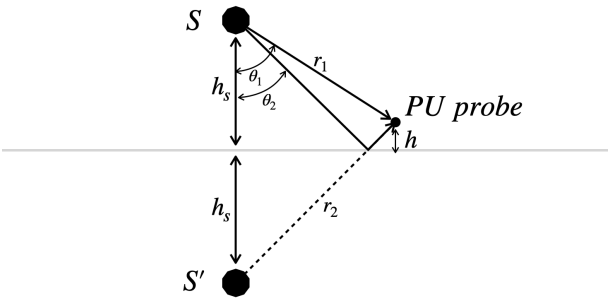

Figure 3.1 Mirror Source Model

At the measurement position, the specific acoustic impedance becomes

$$Z_m = \frac{p_{tot}}{u_{n,tot}} = \frac{\frac{e^{-ikr_1}}{r_1} + R\frac{e^{-ikr_2}}{r_2}}{\frac{e^{-ikr_1}}{r_1}\left(1 + \frac{1}{e^{ikr_1}}\right)\cos(\theta_1) - R\frac{e^{-ikr_2}}{r_2}\left(1 + \frac{1}{e^{ikr_2}}\right)\cos(\theta_2)}\rho_0 c_0 , \qquad (3.9)$$

being r_1 the distance from the probe to the source, r_2 the distance from the probe to the mirror source, and h_s the distance from the source to the surface. Considering a normal incidence angle and equation, the planar reflection coefficient and surface impedance are calculated as

$$R = e^{-ik(r_1 - r_2)}\frac{r_2}{r_1}\frac{Z_m - 1}{Z_m\frac{r_1}{r_2}\frac{ik_0 r_2 + 1}{ik_0 r_1 + 1} + 1} \qquad (3.10)$$

$$Z_s = \frac{1 + R}{1 - R}\frac{ik_0 h_s}{ik_0 h_s + 1}, \qquad (3.11)$$

in which the distance from the probe to the mirror source becomes $r_2 = r_1 + 2h$. This method accounts for the proximity of the source to the sample, while considering a planar reflection

coefficient. Other methods that correct for spherical reflections have been developed by means of iterative algorithms, taking as input the impedance measured by the mirror source [23]. These methods have achieved improved results at lower frequencies under anechoic conditions; however, the mirror source model has proven to be still more robust under in-situ conditions [21, 25, 28], while not requiring large samples to prevent edge effects [5]. This model has been found to be insensitive to the environment when reflective surfaces are located further than 1.5m from the probe, valid for a source-to-probe distance of the system used, of $\mathrm{r} = 26\mathrm{cm}$ [31].

Another simplification taken by these models is the normal transmission assumption, which limits the applicability to normal incidence angle measurements for porous materials that can be classified as bulk or extended reactive. The following subchapter will explain further details on this topic and its implication on the absorption coefficient.

3.3.5 Sample size

The formulations mentioned above assume a sample of infinite extension, for which the size effect becomes problematic for reduced sample sizes. This is caused due to the diffraction of the waves at the edges of the sample, interfering both constructively and destructively at the probe location [23]. A solution has been proposed by implementing a half-space sound field model based on the Boundary Elements Method [32]. Promising results have been obtained numerically and experimentally in samples as small as $200x200\mathrm{mm}^2$, being insensitive to the sample size and PU probe measuring position. However, this method requires the sample to be flush-mounted on a rigid surface. This necessitates specific conditions for sample preparation and laboratory mounting, thus falling outside the in-situ category. Moreover, previous studies have focused on the sample size effect, mainly on single materials or under anechoic conditions [23, 27].

3.4 LOCAL AND EXTENDED REACTIVE MATERIALS

When the ratio of wavenumbers at the transmitted and incidence media, known as the refraction index, is large, the transmission angle approaches 0. This implies that, due to refraction, regardless of the incident wave, the transmitted wave propagates normally with respect to the surface of the material. In some porous media, this can occur due to a lower sound speed in comparison with the air. This is referred to as local reaction, also known as normal or point reacting, by the fact that the acoustic properties depend on local conditions.

The local reaction assumption enables us to characterize a material's surface in terms of a normal incidence surface impedance, thus allowing us to derive expressions to describe the reflected and absorbed energy [4]. However, not all materials can be assumed to behave locally reacting, which can be the case of fibrous materials with low flow resistivity [33] or backed by an air cavity [22]. These materials are denoted as Extended Reactive, non-local, or Bulk reacting, implying a tangential propagation within the medium and, thus, the acoustic properties at a point are no longer dependent only on local conditions.

Given Snell's equation (2.18), at nearly normal incidence, both incident and transmitted angles are equal to 0, resulting in identical results for both local and extended models. Thus, measurements with an impedance tube or with a PU at normal incidence with the sound field models described in section (3.3.4) yield accurate results, disregarding the material's properties.

Mathematical models of the sound field above a non-locally reactive material must be considered when taking measurements at a non-normal incidence angle [33]. For increasing oblique incidence angles, results from both methods are expected to differ as the angle increases. The local-reaction assumption can lead to an underestimation of the random incidence absorption coefficient when measuring bulk reaction samples. However, this difference becomes smaller as the flow resistivity and thickness of the material increase. Similarly, increasing the thickness of the sample produces a similar effect [22].

3.5 CONVERSION BETWEEN ABSORPTION COEFFICIENTS

In 1928, E.T. Paris found a relation from reverberation theory between the random incidence absorption coefficient α_d, also referred to as diffuse field, and the absorption coefficient at an incident angle $\alpha(\theta_i)$. This coefficient can be defined theoretically by averaging the oblique absorption coefficient over all incident angles, assuming equal probability [34]

$$\alpha_d = 2\int_0^{\pi/2} \alpha(\theta_i)\sin(\theta_i)\cos(\theta_i)\mathrm{d}\theta_i = \int_0^{\pi/2} \alpha(\theta_i)\sin(2\theta_i)\mathrm{d}\theta_i \,. \tag{3.12}$$

Additionally, London [35] developed formulations to predict reverberant sound absorption coefficient from the normal incidence values α_n, using star-type statistics and assuming local reaction

$$\alpha_d = 8\left[\frac{1-\sqrt{1-\alpha_\mathrm{n}}}{1+\sqrt{1-\alpha_\mathrm{n}}}\right]^2\left[\frac{2}{1-\sqrt{1-\alpha_\mathrm{n}}} - \frac{1-\sqrt{1-\alpha_\mathrm{n}}}{2} - 2\ln\left[\frac{1-\sqrt{1-\alpha_\mathrm{n}}}{2}\right]\right]. \tag{3.13}$$

Different authors have studied the translation from impedance tube measurements to reverberant chamber method, finding discrepancies between the measured and the translated coefficient using formulations due to factors such as excess absorption due to edge-effect, reduced or excess of absorption due to the lack of diffusion and mounting conditions [5]. To account for the edge effect caused by the finite sample size, a theoretical formulation based on a variational approach was developed [36], which relies on the computation of a Radiation Impedance, Z_R. Simplified for rectangular samples with dimensions a and b, it can be obtained by

$$\mathrm{Z_R}(\theta_\mathrm{i},\phi) = \frac{\mathrm{jZ_0k_0}}{2\pi\mathrm{ab}}\int_0^\mathrm{a}\int_0^\mathrm{b} 4\cos(\mathrm{k_0}\mu_\mathrm{x}\kappa)\cos(\mathrm{k_0}\mu_\mathrm{y}\tau)\frac{\mathrm{e}^{-\mathrm{jk_0}\sqrt{\kappa^2+\tau^2}}}{\sqrt{\kappa^2+\tau^2}}(\mathrm{a}-\kappa)(\mathrm{b}-\tau)\mathrm{d}\kappa\mathrm{d}\tau \qquad (3.14)$$

As the radiation impedance depends only on the sample dimensions, angles of incidence, and frequency, some approximations have been proposed, enabling interpolation to a wide frequency range [37]. By means of this approach, translation between infinite to finite, and finite to infinite sample sizes can be performed, finding good agreement to numerical and experimental data [38].

4 METHODOLOGY

Diffuse field measurements are conducted employing the reverberant chamber method, whereas impedance tube and PU Probe techniques are employed for normal incidence measurements. Given the absence of an established methodology for the PU Probe, a sensitivity analysis is performed. Reference curves are established through supplementary flow resistivity measurements, whose methodology is outlined as well. Subsequently, the fitting procedure and a methodology for comparing absorption coefficients under both diffuse and normal incidence conditions are presented. Measurement results and comparisons are then described in chapter 5.

4.1 MATERIALS TO STUDY

Melamine foam and rockwool were chosen for this study due to their availability and cost-effectiveness as sound-absorbing materials. Other materials with elevated costs were excluded as the reverberant chamber method requires a significant testing area. For melamine foam, all main parameters were previously measured through direct experimental methods [38]. Two thicknesses and two densities were considered with the rockwool, from which only a reference range of flow resistivity was available from the manufacturer (Table 4.1). Thus, additional flow resistivity measurements are to be performed, enabling the modeling of these materials.

Table 4.1 Reference macroscopic properties of the selected materials

	h[mm]	$\rho\left[\frac{kg}{m^3}\right]$	$\sigma\left[\frac{Ns}{m^4}\right]$	ϕ [−]	α_∞[−]	Λ [μm]	Λ' [μm]
Melamine	50	9.6	12220	0.98	1.01	115	116
Rockwool	50	55	> 15000				
		70	> 20000				
	100	55	> 15000				
		70	> 20000				

4.2 FLOW RESISTIVITY

The flow resistivity of the selected materials was measured using the alternating airflow method, following the standard ISO 9053 [6]. The next sections describe the conditions under which the measurements were conducted.

4.2.1 Measurement conditions and equipment

The measurement system consists of a loudspeaker connected to a membrane to produce an alternating airflow, from which the displacement of the piston is measured by an accelerometer. The cavity excited by the piston is enclosed by the sample, fixed by a sample holder, and sealed. The pressure in the cavity is then measured with a microphone. The equipment used consisted of: GRAS 40AE microphone with preamplifier type 26CA, sound calibrator Nor1256, accelerometer PCB model 352C33, B&K calibration exciter type 4294, wax, NI USB-4431 signal acquisition system, alternating airflow measurement system, and a laptop with MATLAB installed (Figure 4.1).

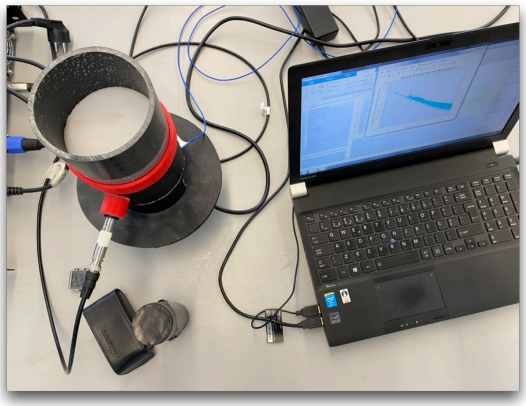

Figure 4.1 Airflow resistivity measurement setup

4.2.2 Size, arrangement and assembly of the samples

The 50mm thick samples from the 100mm diameter impedance tube measurements were used for this procedure. Additional rockwool samples had to be taken since this material tore apart easily. Three or more specimens from each material were tested, following the standard.

4.2.3 Procedure

Both microphone and accelerometer were calibrated, and the sensitivity values were recorded. Once calibrated, they were fixed into position. The accelerometer was fixed to the piston surface using wax. The specimens were fitted snuggly into the sample holder, ensuring no compression and a good seal of the sample holder. Following equation (2.8), the flow resistivity was calculated as

$$\sigma = \frac{\mathrm{A} \cdot \mathrm{p_{ref}} 10^{\mathrm{SPL}/20}}{2\mathrm{d}\pi\mathrm{f}\frac{\mathrm{A_p h_p}}{2\sqrt{2}}} \tag{4.1}$$

where $\mathrm{p_{ref}} = 2 \cdot 10^{-5}\ Pa$ is the reference pressure, SPL is the RMS sound pressure level measured in dB, Ap is the piston area, and $\mathrm{h_p}$ is the RMS peak-to-peak displacement of the piston. The measurements uncertainty is then calculated by considering a 2% deviation from the piston and sample diameter, sample thickness, pressure level measured, and 10% from the peak-to-peak displacement of the piston.

4.3 IMPEDANCE TUBE

The selected materials were measured in the Impedance Tubes of the Department of Civil Engineering (DEC) of the University of Coimbra (Portugal), following the standard ISO 10532-2 [17]. The next sections describe the conditions in which the measurements were conducted.

4.3.1 Measurement conditions and equipment

The impedance tubes of DEC have 100mm and 38mm of diameter, with a working frequency range of 50Hz-1.6kHz and 200Hz to 5kHz, respectively. The lower frequency limit is obtained from the microphone spacing, and the upper limit is determined by the tube diameter. The equipment used was the following: Impedance tubes, samples, 2 microphones GRAS type 46AE, sound source, amplifier M700, NI USB-4431 signal acquisition system, and a Laptop with Matlab (Figure 4.2).

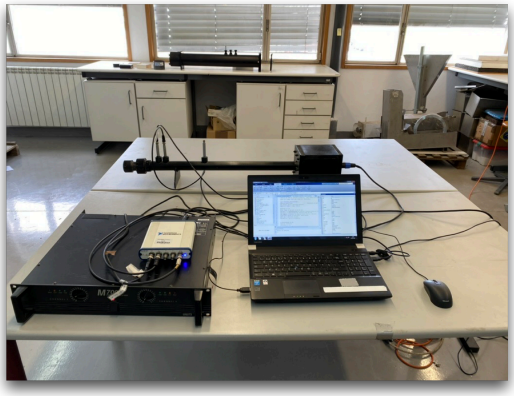

Figure 4.2 Impedance Tube measurement setup (left). Representative specimens of melamine and rockwool in 100mm and 38mm diameter (right)

4.3.2 Size, arrangement and assembly of the samples

Multiple specimens were obtained for each of the materials, for the small tube and for the large tube, using a sharpened PVC tube with the dimensions of the tubes. Care was taken not to compress or deform the material, especially in the case of the rockwool. This material was noted to tear apart easily while cutting the 38mm samples. Samples were placed in the sample holding a firm tight fit, ensuring that the front was perfectly normal to the tube axis.

4.3.3 Procedure

The transfer-function method described in ISO 10532-2 [17] was followed, which relies on the obtention of a transfer function between two positions in front of the sample to obtain the normal incidence reflection coefficient. This is obtained by

$$R = \frac{H_{12} - e^{-jk_0 s}}{e^{jk_0 s} - H_{12}} e^{2jk_0 x_1}, \tag{4.2}$$

where H_{12} is the complex acoustic transfer function between the two microphone positions, s is the distance between the microphones and x_1 is the distance between the sample and the further microphone location. The transfer function is estimated by using the function “tfestimate()” in Matlab. Since the two-microphone technique was used, a calibration factor is computed to correct for microphone mismatch. This enables the subsequent calculation of the absorption coefficient and the specific acoustic impedance. Repeated measurements using the same mounting conditions were performed on the specimens, and the combined absorption curve from both tubes was obtained by averaging over the overlapping frequency range of both tubes.

4.4 PU PROBE

The selected materials were measured using a PU Probe on the premises of Amplitude Acoustics, located in Maia, Portugal. The subsequent sections detail the conditions under which measurements were performed.

4.4.1 Measurement conditions and equipment

Measurements were performed inside an empty office space ($\approx 30m^2$), with no acoustic treatment other than acoustic ceiling tiles. The following equipment used included: Microflown Insitu Impedance Setup, tripod, measuring tape, Scout Data acquisition system, MFPA-2 signal conditioner, and laptop with Velo Software (Figure 4.3).

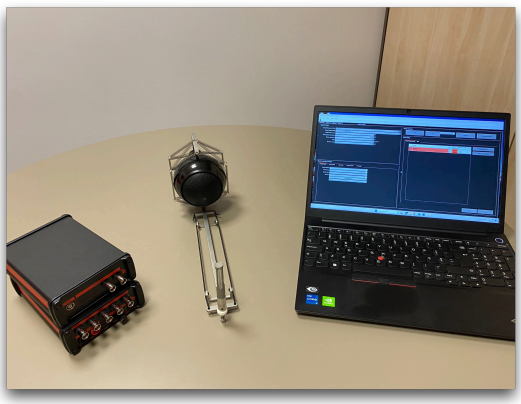

Figure 4.3 PU Probe measurement equipment

4.4.2 Sensitivity Analysis

To gain confidence in measuring with the PU Probe, the influence of some parameters was first analyzed. This analysis aims to provide answers regarding the minimum sample size, the calculation method, and the receiver position. The results of both materials studied, melamine and rockwool, were then compared, enabling to establish general guidelines for future in-situ measurements on porous materials. For this study, 50mm thick rigidly backed samples of Melamine foam and Rockwool PN70 were selected, with the aim to represent a wider range of flow resistivity materials.

To simplify the analysis, certain factors were held constant throughout this study, including the probe-to-sample distance, the measurement environment and the calibration technique, following the conclusions from previous research work and practical experience using the PU Probe technique for absorption measurements.

To quantify the difference between the measured absorption coefficients, α_{meas}, and the reference absorption curve from the Equivalent Fluid models, α_{ref}, the mean error was calculated as

$$e = \frac{1}{N_b}\sum_{k=1}^{N_b}\left|\frac{\alpha_{\text{meas},k^{th}band} - \alpha_{ref,k^{th}band}}{\alpha_{ref,k^{th}band}}\right| \tag{4.3}$$

where N_b denotes the number of one third-octave bands considered. The reference absorption curve was obtained through the JCA model, for melamine, and through the DBM model, for rockwool. For this analysis, the frequency range was subdivided into two subranges, covering the one third-octave bands within a medium frequency range (400-800Hz), and a higher frequency range (800-10kHz). For comparison, the same error analysis is performed on the Impedance Tube measurements.

4.4.3 Procedure

PU probe measurements were conducted at normal incidence, employing a tripod setup with the probe positioned 5mm away from the sample's surface (Figure 4.4). The calibration followed the free-field calibration method outlined in section 3.3. The sample sizes varied, ranging from sizes larger than 1m² to as small as 200x200mm². Measurements were taken at both central and at the "confidence region" [23]. Surface impedance was determined through both the Plane Wave Method (PW) and the Mirror Source Method (MS). Results of this analysis are further presented in section 5.3.

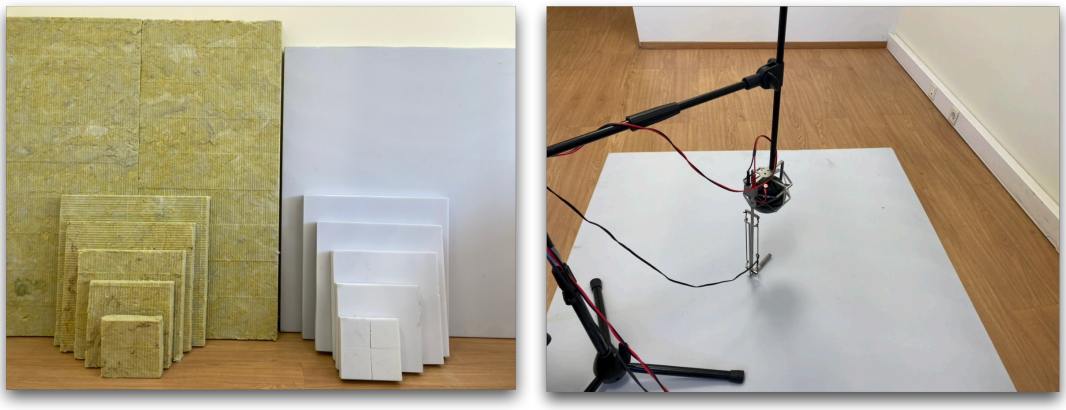

Figure 4.4 Specimens used for sensitivity analysis (left), measurement on large melamine sample (right)

4.5 REVERBERANT CHAMBER

The selected materials were measured in the Reverberant Chamber of the Department of Civil Engineering (DEC) of the University of Coimbra (Portugal), following the standard ISO 354:2003 [14]. The subsequent sections detail the conditions under which measurements were performed.

4.5.1 Measurement conditions and equipment

The Reverberant Chamber of DEC has a volume of $V = 125m^3$ and total surface area of $S_t = 158m^2$. It contains 5 fixed acoustic diffusers positioned on the ceiling and one on the floor Figure 4.6. During the studies, it was observed, when performing the measurements in the reverberant chamber, that the measurements considering the minimum sample size required by the standard ($10m^2$) yielded a pronounced decrease in sound absorption above 800 Hz (Figure 4.5), which was present for all materials. This could be attributed to the smaller volume of the acoustic chamber and the positioning of the diffusers, which were predominantly concentrated on the ceiling.

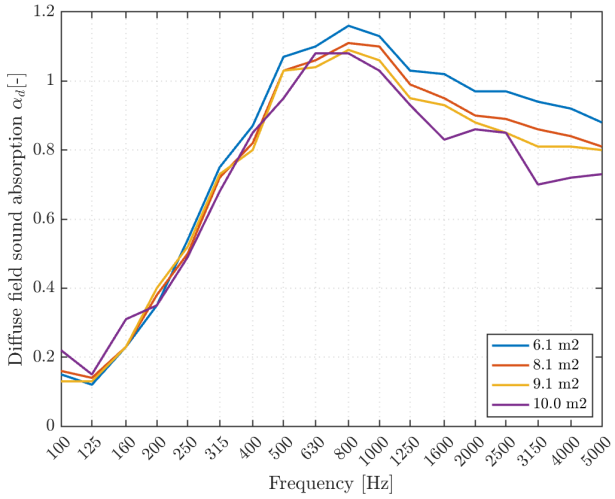

Figure 4.5 Sample size comparison on melamine samples

By decreasing the sample size by a factor of $(V/200)^{3/2}$, suggested originally by the standard for large chamber volumes, a corresponding sample size is found to be between 7.2m^2 and 8.72m^2 for the volume of the reverberant chamber in use. Given the specimen sizes, a sample area of 8.1m^2 was chosen for all subsequent measurements. The equipment used was the following: Calibrator B&K type 4231, microphone G.R.A.S type 46AE, Power Amplifier B&K type 2716, measuring tape, 01dB DO12 dodecahedron sound source, Laptop with the software dBBati32, and a Symphonie acquisition unit.

4.5.2 Size, arrangement and assembly of the sample

Following mounting type A (according to annex B of standard ISO 354 [14]), the sample was positioned on the floor of the chamber, and two reflective wooden frames of heights 50mm and 100mm were built to cover the edges for both material thicknesses to avoid absorption from the sample's sides.

The Rockwool and Melamine samples were positioned inside the frame, ensuring an exposed sample area of $S = 8.1m^2$, fulfilling the standard's minimum area requirement by the factor of volume applied (Figure 4.6). Care was taken not to leave any air gap between the sample and the frame nor between the sample and the floor.

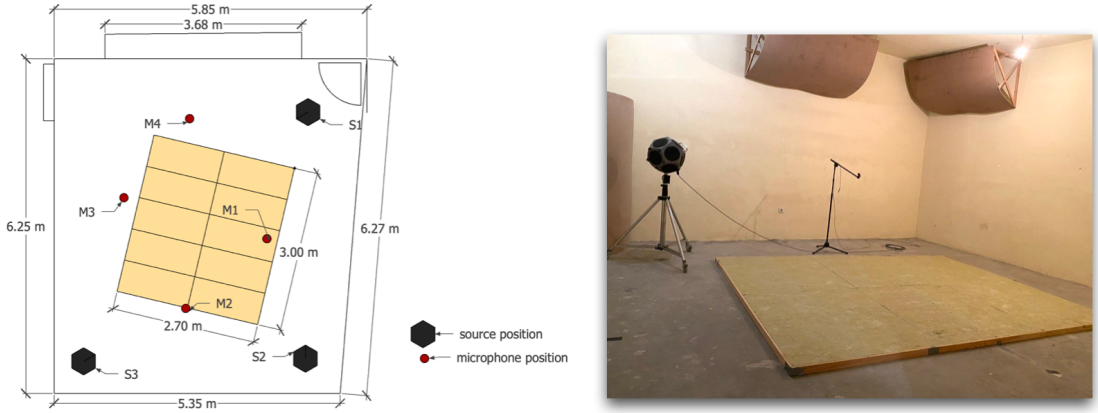

Figure 4.6 Measurement configuration (left). Rockwool sample of 8.1 m^2 inside of the frame (right)

4.5.3 Procedure

The reverberation time of the reverberant chamber was measured using a Maximum Length Sequence (MLS) signal, first in the empty chamber and then with the material installed with the reflective frame. Sabine's equation was used to obtain the equivalent sound absorption area A_T,

$$\mathrm{A_T} = \mathrm{A_s} - \mathrm{A_e} = 55.3\mathrm{V}\left(\frac{1}{\mathrm{c_s T_s}} - \frac{1}{\mathrm{c_e T_e}}\right) - 4\mathrm{V}(\mathrm{m_s} - \mathrm{m_e})\,, \tag{4.4}$$

where $\mathrm{T[s]}$ stands for the reverberation time, $\mathrm{m[m^{-1}]}$ is the power attenuation coefficient, and the prefixes "s" and "e" represent the measurements with the sample and empty chamber, respectively. The temperature and relative humidity were measured for both $\mathrm{T_s}$ and $\mathrm{T_e}$. The sound absorption coefficient is then obtained by the ratio $\alpha_s = \mathrm{A_T}/S$. Measurements were performed with 4 microphone positions, ensuring at least 1.5m between them, 2m to the source, and 1m to any wall and sample. The sound source was positioned at 3 locations, with at least 3m of

separation, ensuring measurement points, as shown in Figure 4.6. The sound absorption coefficient α_s is obtained for all 1/3 octave band central frequencies from 100 to 5000, as required in ISO 354 [14].

4.6 MODEL FITTING

A model fitting procedure is proposed to overcome the limitation within the lower frequency range of the PU Probe measurements. This procedure serves a dual purpose: first, to yield a comprehensive broadband absorption curve, and second, to estimate the diffuse field absorption coefficient using Paris equation (3.12) from both PU Probe and Impedance Tube measurements. The validation of this procedure will be achieved by comparing the inverse parameters obtained with the experimental values.

The inverse methodology was implemented using MATLAB's "fmincon" function within a Globalsearch optimization algorithm, solving for the global minimum of the objective function, defined here as the absolute error between the measured and the reference absorption coefficient from the equivalent fluid model

$$F(f, h, \sigma, \phi, \alpha_\infty) = \sum_{fl}^{fu} |\alpha_{PU,Tube}(f) - \alpha_{ref}(f, h, \sigma, \phi, \alpha_\infty)| \,. \tag{4.5}$$

Globalsearch uses a scattered search mechanism to generate starting points within the search space of the variables of the function [39]. MATLAB's Multistart algorithm was also tested, which uniformly distributes starting points within bounds. However, the Globalsearch algorithm was preferred, avoiding the need of defining a fixed number of starting points.

Two reference models already described, DBM and JCA, were implemented in the algorithm to obtain the reference absorption coefficient. The former has the advantage of only depending on a single variable. However, if global minima can be obtained by the optimization algorithm, more parameters can be retrieved by using the JCA model as a reference. The characteristic lengths were estimated from the variable parameters by equation (2.12). Search space bounds for the flow resistivity, porosity and tortuosity were defined, covering a wide range of porous materials (Table 4.2). The thickness h of the material can also be considered variable within an established range, such as in cases when the thickness is unknown. Since the material's thickness is well established, it was left constant for this study.

Table 4.2 Search space boundaries of the optimization variables

	$\sigma\left[\frac{Ns}{m^4}\right]$	$\phi\ [-]$	$\alpha_\infty[-]$
Lower bound	1 x10^3	0	1
Upper bound	2 x10^5	1	5

This inverse characterization was performed for both the Impedance Tube and PU probe measurements, enabling a comparison between the retrieved parameters from both methods to the parameters using direct experimental techniques. The frequency range's lower and upper bounds, fl and fu, respectively, were defined from 100Hz to 5000Hz in the case of the impedance tube. For the PU Probe measurements, these limits are to be defined following the sensitivity analysis results.

4.7 COMPARISON BETWEEN METHODS

To allow a comparison between the three methods studied, the measured data was treated following the considerations presented next.

4.7.1 Conversion into random incidence

By means of the proposed inverse characterization procedure, the retrieved characteristic impedance and complex wavenumber can be utilized to estimate the absorption coefficient in a virtual diffuse field using equation (3.12), achieved by trapezoidal numerical integration, with $\Delta\theta = \pi/1000$, being $\alpha(\theta_i)$ calculated for incidence angles from 0 to $\pi/2$. These results are then compared to the curve obtained from the simplified London's equation derived directly from the absorption coefficient values obtained under normal incidence.

4.7.2 Reverberant chamber non-diffuseness

Addressing the lack of diffuseness of the acoustic chamber was done by considering a smaller sample size of 8.1m^2, accounting for the reduced volume of the chamber as discussed in section (4.5.1). As mentioned, this effect was predominant at higher frequencies. While a decrease in sound absorption at high frequencies is still visible, further attempts to increase diffusiveness by the installation of additional acoustic diffusers was out of the scope of this work.

4.7.3 Conversion from finite to infinite sample size

To correct for the excess absorption from the reverberant chamber measurements, the measured Sabine's absorption coefficient α_s is converted into a virtual infinite sample size by applying a sample size correction, considering the real part of the radiation impedance Z_R

$$\alpha_{\infty} = \frac{\alpha_s}{\frac{1}{\pi}\int_0^{\pi/2}\int_0^{2\pi}\frac{\sin\theta}{\mathrm{Re}(Z_R)}\mathrm{d}\phi\mathrm{d}\theta}. \quad (4.6)$$

This correction was obtained by the polynomial regression approach detailed in [40].

5 RESULTS AND DISCUSSION

The results obtained following the methodology developed in the previous section are presented as sound absorption coefficients to deliver a compact presentation and to enable comparison with the reverberant chamber method.

5.1 FLOW RESISTIVITY

Table 5.1 displays the measured flow resistivity values and their estimated expanded uncertainties, adhering to ISO 9053 [6] and the GUM method [41], respectively. Reference resistivity values for melamine foam (obtained previously [38]) and rockwool (manufacturer-provided) are also shown for comparison. The acquired values for all materials conformed to the anticipated reference ranges. Consequently, these measurements enabled to obtain reference absorption curves for rockwool using the DBM model.

Table 5.1 Reference and measured flow resistivity values for melamine and rockwool

	$\rho\left[\frac{kg}{m^3}\right]$	$\sigma_{ref}\left[\frac{Ns}{m^4}\right]$	$\sigma_{meas}\left[\frac{Ns}{m^4}\right]$
Melamine	9.6	12220	12227 ± 1251
Rockwool	55	> 15000	20798 ± 2121
	70	> 20000	30869 ± 3148

5.2 IMPEDANCE TUBE

Following ISO 10532-2 [17], the normal incidence sound absorption was obtained for all the tested materials. Figure 5.1 shows the results obtained for melamine foam. The provided data from the manufacturer is plotted as well. Both measured and manufacturer curves show an excellent agreement to the reference curve, obtained from the JCA model using the reference parameters.

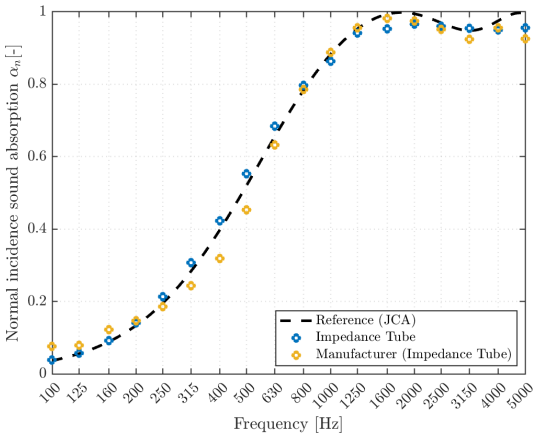

Figure 5.1 Impedance tube measurements on melamine foam, 50mm thickness

No manufacturer data was available for rockwool for normal incidence. Consequently, and to prevent redundant figures, the findings of these samples are further shown in section 5.6.1, where a comparison between Impedance Tube and PU Probe results is conducted.

5.3 PU PROBE SENSITIVITY ANALYSIS

Results considering the calculated mean error from the reference absorption curves (equation (4.3)), averaged over all sample sizes are summarized in Table 5.2. Detailed results for both materials at the largest and smallest sample sizes can be found in the Appendix section, from A - 1 to A - 4.

Regarding the model used to retrieve the surface impedance, in overall, both Mirror Source (MS) and Plane Wave (PW) models yielded equivalent results at higher frequencies. Below 800 Hz, higher errors were found, varying significantly depending on the model, the probe location and the sample size. Values below 300 Hz were not considered valid, given the frequency range of the system used, being primarily limited in the lower boundary of this range by the assumption of plane waves propagating inside of the material, and signal-to-noise ratio issues encountered at the pressure and particle velocity sensors [21].

Table 5.2 Relative error over all sample sizes with PU Probe

	Melamine				Rockwool PN70			
	Center		Conf		Center		Conf	
	PW	MS	PW	MS	PW	MS	PW	MS
400-800Hz	12%	11%	12%	15%	16%	16%	21%	24%
800-10000Hz	1%	1%	1%	1%	2%	2%	2%	3%

In contrast to numerical outcomes assuming free-field conditions, measuring at the on-center position yielded lower errors compared to measurements within the "confidence region." One possible answer to this might be the fact that the results were obtained under different conditions, including different sound field model, and the fact that the sound source was moved together with the sensor. Regardless of these factors, above 800 Hz, the error fell in average within 3% for both materials, down to 200x200mm^2 sample sizes (Table 5.2). For comparison, using the Impedance Tube method with the same reference curves from the Equivalent Fluid models, the mean error found did not surpass 10% error even in lower frequency range (Table 5.3). However, above 800 Hz measurements with the PU Probe yielded a smaller errors than the Impedance Tube.

Table 5.3 Relative error, Impedance Tube

	Melamine	Rockwool PN70
400-800Hz	5%	9%
800-5000Hz	2%	4%

Greater deviations in the form of underestimated absorption at normal incidence were found mainly below 800Hz, resulting in increasing error as the sample size decreases. Figure 5.2 shows the sound absorption coefficient measured at each sample size using the MS model. It can be pointed out that as the sample size increases, it is able to retrieve a more accurate absorption curve down to lower frequencies. In the case of melamine, using the largest sample size yielded an error of 3% at the 630 band while surpassing 10% when measuring with the smallest sample size.

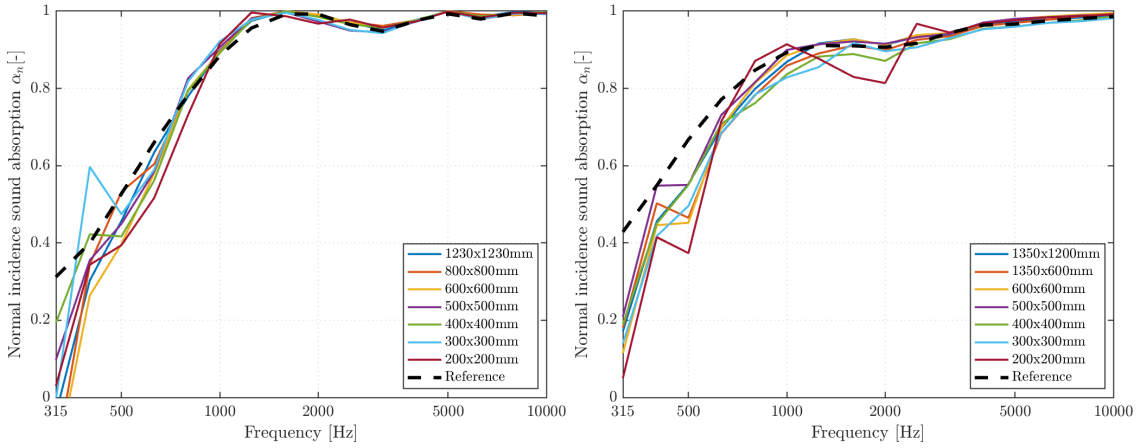

Figure 5.2 Sample size effect on the absorption coefficient for melamine (left) and rockwool (right)

Following these results, further measurements using the PU Probe were performed using the largest sample size, the Mirror Source model and the probe location was fixed in-center, unless

otherwise stated. A summary of these results, meant to guide future in-situ measurements using the PU Probe, can be found in Appendix A - 5.

5.4 REVERBERANT CHAMBER

The results of the measured Sabine Absorption Coefficient measured using the established sample area (8.1m^2) are shown in Figure 5.3 to Figure 5.5. Good agreement was found between the measured curve and the manufacturers at low frequencies. However, a noticeable underestimation occurred above 1 kHz, present at all measured curves. Although this effect was improved by decreasing the sample size, these results confirm that the chamber's diffusivity could still be inadequate at high frequencies.

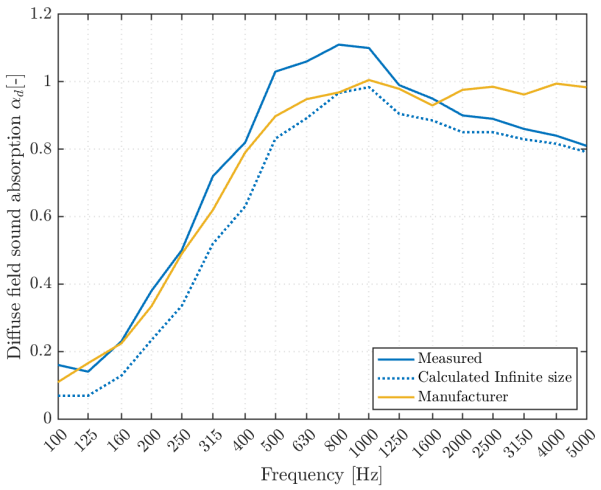

Figure 5.3 Melamine 50mm measured in diffuse field following ISO 354 [14]

By converting the measured absorption curve into one of virtual infinite lateral dimensions, a clear decrease in the absorption is observed. The excess of absorption, which at some frequency bands resulted in absorption coefficients above 1, is effectively addressed. This procedure was especially important for the thicker 100mm samples, where the absorption reached values above 1.2 (Figure 5.4, right). While this procedure is effective in addressing the edge effect, the effect of the lack of diffusion is naturally still present in the calculated infinite size absorption curves.

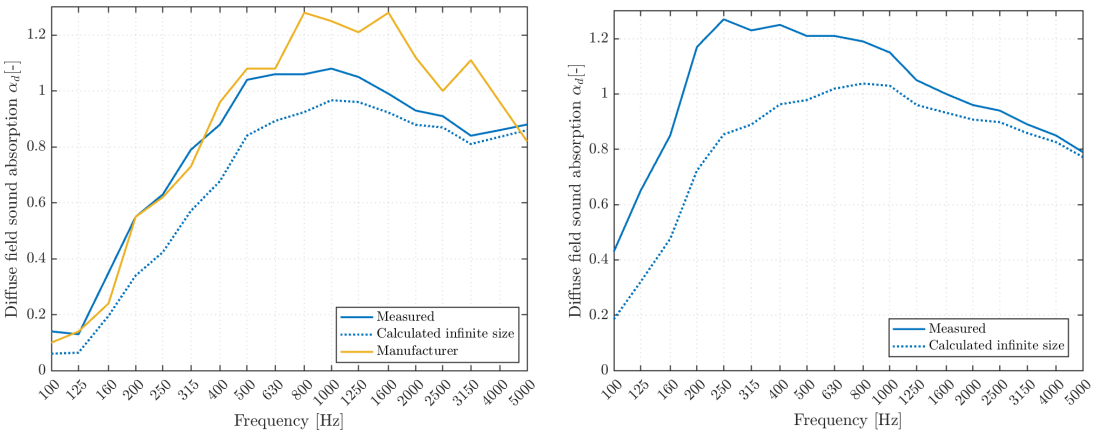

Figure 5.4 Rockwool PN55, 50mm (left) and 100mm (right) thick measured in diffuse field

Similarly to the melamine foam, good agreement is found below 500 Hz, compared to the manufacturer data. However, for rockwool samples, the manufacturer data seems to shows an overestimation of the absorption coefficient, which is especially remarkable for rockwool PN55, reaching values above 1.2. This difference in the manufacturer's measurements suggests that both rockwool materials might have been tested under different measurement conditions. No data for the 100mm materials was available from the manufacturer.

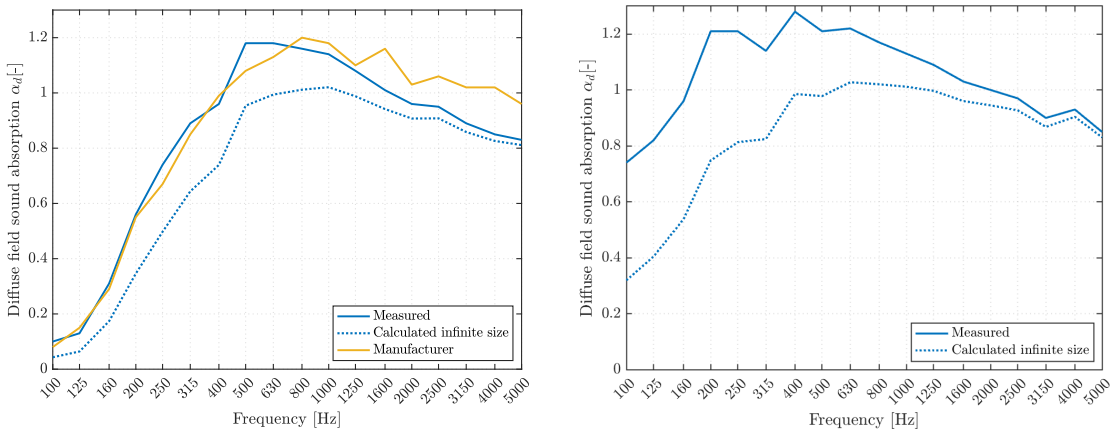

Figure 5.5 Rockwool PN70, 50mm (left) and 100mm (right) thick measured in diffuse field

5.5 MODEL FITTING

5.5.1 Inverse characterization

The parameters of the JCA model were inversely retrieved from both Impedance Tube and PU Probe measurements by means of the proposed model fitting methodology. Following the results from the sensitivity analysis, the model fitting range for the PU Probe measurements was set from 800-10000 Hz. A model fitting using the simpler DBM model was also implemented for comparison. Measured and reference parameters are shown in Table 5.4 and Table 5.5.

Table 5.4 Inverse characterization results of melamine foam

Macroscopic parameters	Reference	Measured	Inverse Tube JCA	Inverse Tube DBM	Inverse PU JCA	Inverse PU DBM
$\sigma\left[\frac{Ns}{m^4}\right]$	12200	12227 ± 1251	11221	12964	12381	11831
$\phi\ [-]$	0.98	-	1	-	0.94	-
$\alpha_\infty[-]$	1.01	-	1	-	1	-
$\Lambda\ [\mu m]$	115	-	114	-	112	-
$\Lambda'\ [\mu m]$	116	-	114	-	112	-

The model fitting algorithm was able to predict accurately the flow resistivity, porosity and tortuosity from both Impedance Tube and PU Probe measurements. The characteristic lengths are also shown, however, they are not variables, but calculated from the variable parameters by equation (2.12). In the case of the Rockwool samples, only the flow resistivity is shown below since there is no reference from the remaining parameters. As can be shown, the resulting flow resistivity estimated fell within the uncertainty range of the measured values.

Table 5.5 Inverse characterization results of rockwool PN55 and PN70

$\sigma\left[\frac{Ns}{m^4}\right]$	Reference	Measured	Inverse Tube AC	Inverse Tube DBM	Inverse PU AC	Inverse PU DBM
$RW\ PN55$	> 15000	20798 ± 2121	19921	21635	18640	19465
$RW\ PN70$	> 20000	30869 ± 3148	28145	27466	30802	30022

5.5.2 Broadband absorption curves

By processing the PU Probe measurements with the proposed model fitting, broadband normal and random incidence absorption curves were obtained. The calculated error decreased significantly, particularly in the lower frequency range, with errors within 5% using the Mirror

Source Model. For a compact presentation, the averaged error over all the measured samples is shown in Table 5.6. These results indicate that, if the model fitting procedure is implemented, regardless of the probe location, the sound field model and using sample sizes as small as 200x200mm^2, accurate results can be obtained.

Table 5.6 Error over all sample sizes, after model fitting procedure

	Melamine				Rockwool PN70			
	Center		Conf		Center		Conf	
	PWA	MS	PWA	MS	PWA	MS	PWA	MS
400-800Hz	8%	5%	6%	5%	2%	2%	2%	3%
800-10000Hz	1%	1%	1%	1%	1%	1%	1%	2%

To avoid redundant plots, results are presented in the following section, in which comparison between all methods is performed. Nonetheless, it can be shown that, even down at the smallest 200x200mm^2 sample sizes, where the size effect introduced the highest errors, the model fittingmethod was able to reconstruct the normal incidence absorption curve down to 100 Hz with good agreement to the reference (Figure 5.6).

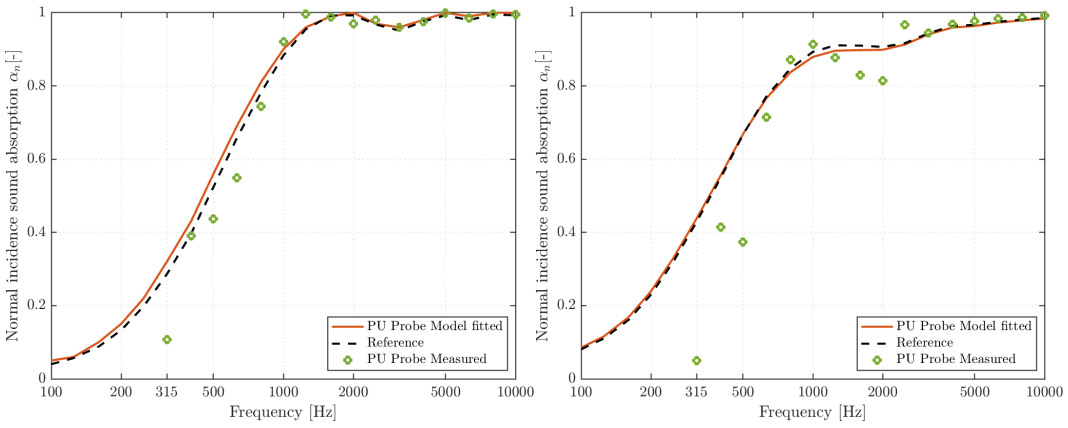

Figure 5.6 Melamine (left) and rockwool (right) results after inverse method, using 200x200mm^2 samples

5.6 COMPARISON BETWEEN METHODS

Methods comparison is divided into normal and random incidence. The former includes Impedance Tube and PU Probe measurements, while the latter encompasses these techniques alongside reverberant chamber measurements.

5.6.1 Normal incidence sound absorption coefficient

The measured normal incidence sound absorption curves from both Impedance Tube and PU Probe methods are presented next, from Figure 5.7 to Figure 5.9, alongside with the retrieved model fitted curve obtained from the PU Probe measurements.

In the case of the melamine foam, both experimental methods show a good agreement with the reference curves from the Equivalent Fluid Models. As noted during the sensitivity analysis, below 800 Hz higher errors were found, which resulted in an underestimation of the absorption coefficient. Below 400 Hz, this underestimation resulted in negative absorption values at the lowest frequency bands, as similarly found in previous works[21] [28]. In the case of melamine, this occurred down to the 315 Hz band.

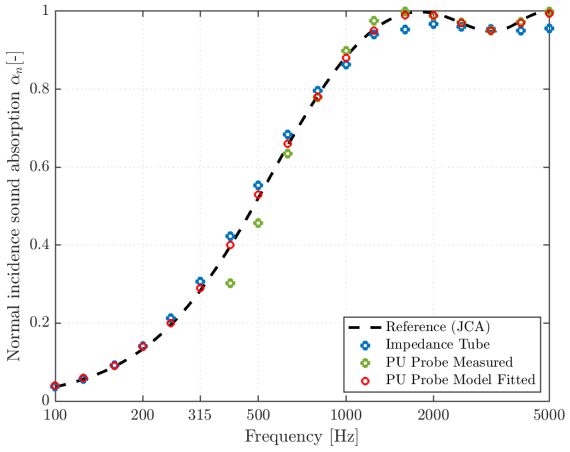

Figure 5.7 Normal incidence measurements of melamine, 50mm thick

The systematic underestimation in the absorption measurements at low frequencies with the PU Probe can be attributed, as mentioned previously, to the limited frequency range of the system used, and to the assumption of plane waves propagation inside of the sample [21]. The PU Probe measurements processed with the proposed model fitting methodology addressed these limitations, obtaining a broadband normal incidence sound absorption curve with good agreement to both impedance tube measurements and the reference curve.

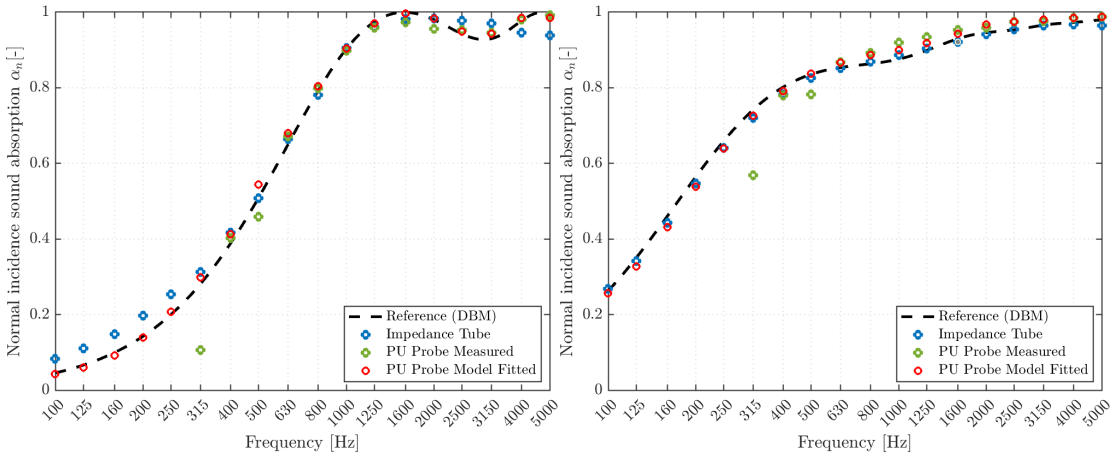

Figure 5.8 Normal incidence measurements of rockwool PN55, 50mm (left) and 100mm (right) thick

Similarly to the melamine foam measurements, good agreement between both techniques and the normal incidence reference curve was found at higher frequencies for all rockwool samples. Unlike the melamine foam measurements, there were no instances of negative absorption values within the valid frequency range of the PU Probe. Nevertheless, underestimated values were observed below 800 Hz. The model fitting performed enabled to obtain comparable results down to 100 Hz from the PU Probe measurements.

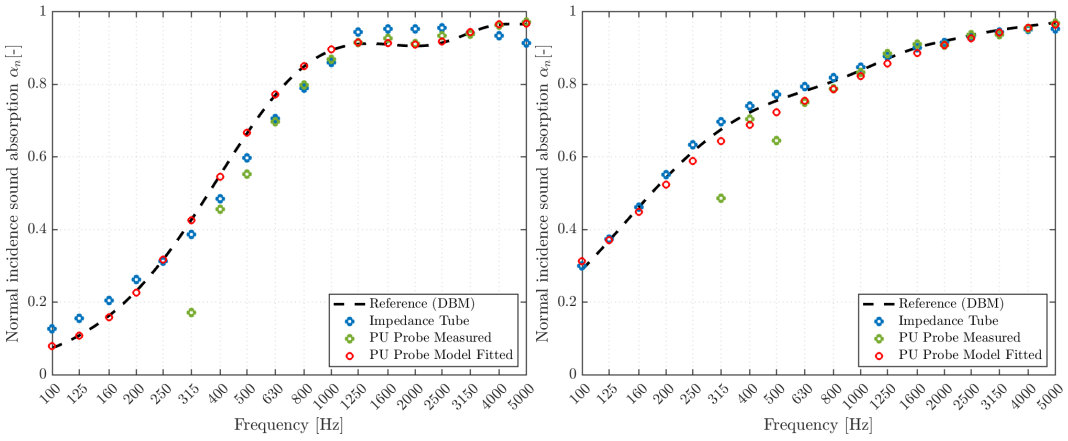

Figure 5.9 Normal incidence measurements on Rockwool PN70, 50mm (left) and 100mm (right) thick

5.6.2 Random Incidence sound absorption coefficient

Following the considerations detailed in section 4.7, the results from the Reverberant Chamber, Impedance Tube and PU Probe are compared for the selected materials, shown in Figure 5.10 for melamine foam and Figure 5.11 to Figure 5.12 for rockwool. As a reference, an analytical curve was obtained using the JCA and DBM models with the reference non-acoustical properties and converted into random incidence through Paris equation.

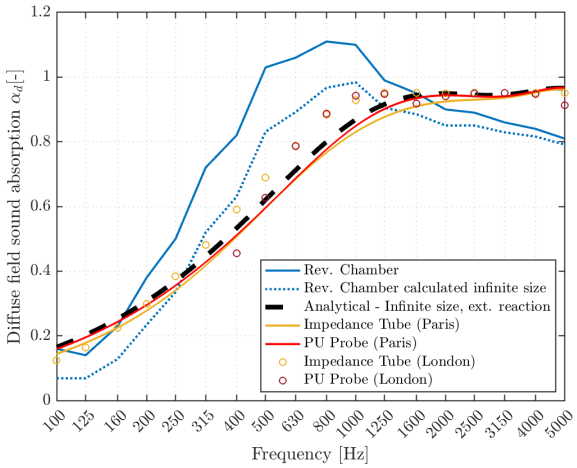

Figure 5.10 Comparison between all methods of melamine foam, 50mm thick

Using London's equation, the simplified conversion to random incidence yielded a fair approximation to the analytical curve. At mid-frequencies, the sound absorption coefficient was over-estimated by the local reaction assumption, particularly in the case of the thin materials with low flow resistivity, such as the case of the melamine foam and rockwool PN55 of 50mm thickness. A better agreement was found for thicker and more resistive samples.

Given the PU Probe's limitation in the low frequency range, London's simplified conversion cannot be obtained directly down to 100 Hz. Values below the working frequency range of the sound source, as well as negative absorption values, were not considered as valid and thus are not converted into random incidence. On other side, the model fitting methodology implementing Paris' equation enabled to obtain a broadband random incidence sound absorption curve for the PU Probe method, down to 100 Hz. Good agreement with the reference curve was found using this methodology from both Impedance Tube and PU Probe, for all materials tested.

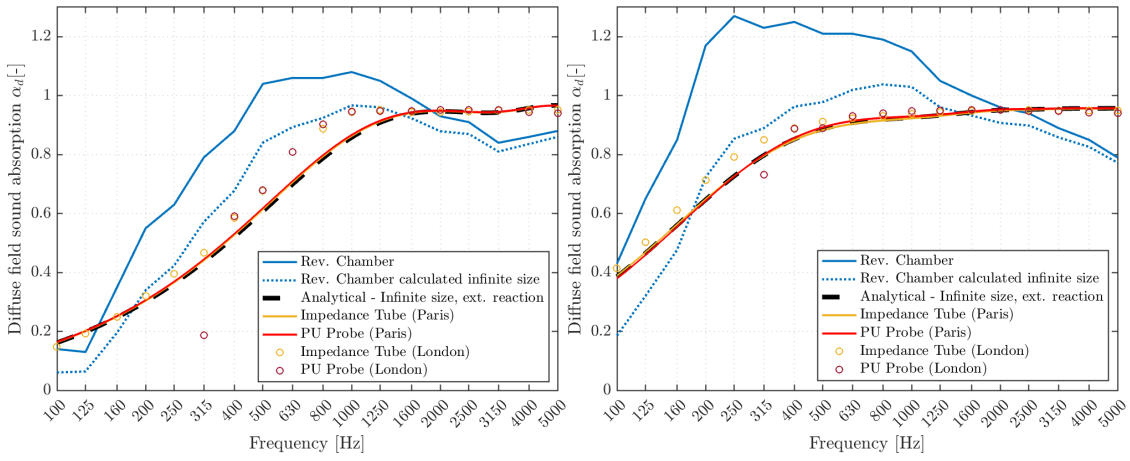

Figure 5.11 Comparison between all methods of Rockwool PN55, 50mm (left) and 100mm (right) thick

In terms of the measured coefficient in the reverberant chamber, the conversion into an infinite size enabled a better comparison to the values from the Impedance Tube and the PU probe, as it reduced the excess of absorption caused from the edges. In comparison with the analytical curve, it is observed that the measured coefficients yield a similar behavior for all the materials tested, oscillating around the reference curve. This can be attributed to the fact that the measured coefficient relies on assumptions regarding the distribution and behavior of sound energy according to Sabine's theory. The lack of diffusion in the measurement chamber further hindered the results from these measurements.

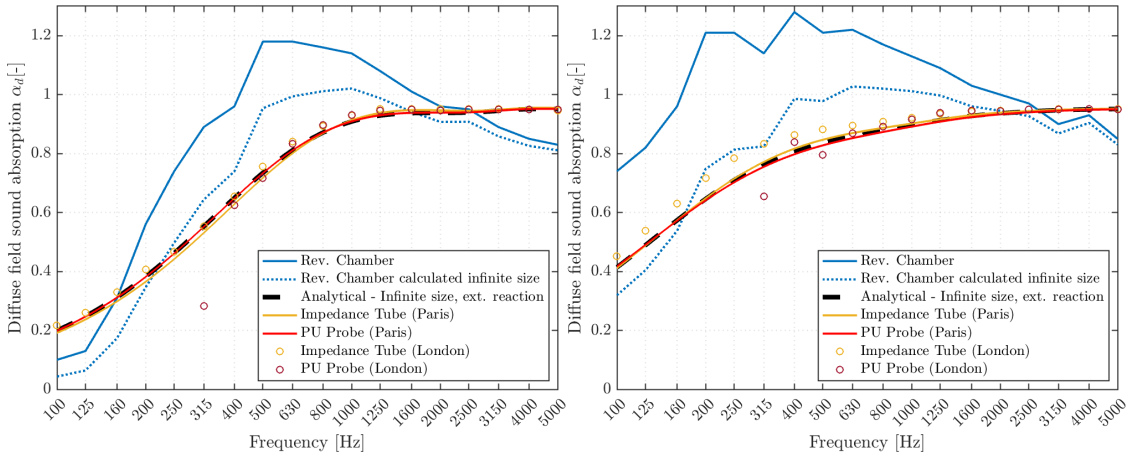

Figure 5.12 Comparison between methods with Rockwool PN70, 50mm (left) and 100mm (right) thick

6 CONCLUSIONS AND FUTURE WORK

This study highlighted the complexity and significance of various factors that come into play whenever performing in-situ measurements of sound-absorbing porous materials with a PU Probe. Below 800 Hz, the effect of sample size, sound field model and probe location proved to be significant on the measured absorption coefficient. Nonetheless, results showed to be very accurate at higher frequencies, yielding errors smaller than those obtained by the impedance tube, in reference to the Equivalent Fluid Models. Taking advantage of this, the model fitting procedure developed proved to be an effective solution to address the higher errors found in the low-frequency region, effectively obtaining broadband absorption curves with samples as small as 200x200mm^2.

By means of the JCA model, the macroscopic parameters inversely retrieved were found in excellent agreement with those obtained by direct experimental methods, thus validating the proposed inverse method. Furthermore, this procedure enabled the calculation of a random incidence absorption coefficient with an angle-dependent surface impedance, becoming thus a

more accurate than the simplified approach using London's equation, which assumes the material as locally reactive.

The size correction methodology proposed by Thomasson [40], implemented on Sabine's absorption coefficient, facilitated the comparisons with the Impedance Tube and PU Probe methods by accounting for the excess absorption due to finite sample size. Nonetheless, a possible poor diffusion of the reverberant chamber hindered comparison with the Impedance Tube and PU Probe techniques. For future absorption measurements, this should be addressed by the addition of hanging acoustic diffusers as well as on the walls, distributed along the volume of the chamber.

The sample size effect has an important influence on the random incidence absorption, for which considering the absorption coefficient using the Transfer Matrix Method or by Impedance Tube or PU Probe measurements will underestimate the sound absorption coefficient of finite sample sizes. It is thus important to consider the dimensions of the material to be characterized, either analytically or by numerical models, before using these values on geometrical acoustic simulation software. For accurate predictions at low frequencies, where phase information on the boundary conditions is required, the use of the complex-valued reflection coefficient or surface impedance is recommended.

Combining calibration techniques, such as using an Impedance Tube calibration along with a free-field technique should be further studied, with the potential to improve the measurements at lower frequencies. For field measurements, however, this would affect the portability of the system. Moreover, more complex systems should be further studied, such as non-flat panels or materials with air gaps. Regardless of its limitations, valuable information from the sound-absorbing porous materials can be retrieved non-destructively and in-situ in a wide frequency range using a PU Probe along with an inverse characterization post-processing. However, careful consideration of the factors mentioned should be taken.

REFERENCES

[1] N. H. Bhingare, S. Prakash, and V. S. Jatti, "A review on natural and waste material composite as acoustic material," *Polymer Testing,* vol. 80, p. 106142, 2019.

[2] K. Hirosawa, K. Takashima, H. Nakagawa, M. Kon, A. Yamamoto, and W. Lauriks, "Comparison of three measurement techniques for the normal absorption coefficient of sound absorbing materials in the free field," *The journal of the acoustical society of America,* vol. 126, no. 6, pp. 3020-3027, 2009.

[3] J. Allard and N. Atalla, *Propagation of sound in porous media: Modelling Sound Absorbing Materials*. John Wiley & Sons, 2009.

[4] F. J. Fahy, *Foundations of engineering acoustics*. Elsevier, 2000.

[5] T. Cox and P. d'Antonio, *Acoustic absorbers and diffusers: theory, design and application*. CRC press, 2016.

[6] *Acoustics - Materials for acoustical applications - Determination of airflow resistance*, ISO 9053:1991(E).

[7] O. Doutres, Y. Salissou, N. Atalla, and R. Panneton, "Evaluation of the acoustic and non-acoustic properties of sound absorbing materials using a three-microphone impedance tube," *Applied acoustics,* vol. 71, no. 6, pp. 506-509, 2010.

[8] R. Dragonetti, C. Ianniello, and R. A. Romano, "Measurement of the resistivity of porous materials with an alternating air-flow method," *The Journal of the Acoustical Society of America,* vol. 129, no. 2, pp. 753-764, 2011.

[9] M. E. Delany and E. Bazley, "Acoustical properties of fibrous absorbent materials," *Applied acoustics,* vol. 3, no. 2, pp. 105-116, 1970.

[10] Y. Miki, "Acoustical properties of porous materials-Modifications of Delany-Bazley models," *Journal of the Acoustical Society of Japan (E),* vol. 11, no. 1, pp. 19-24, 1990.

[11] R. Panneton and E. Gros, "A missing mass method to measure the open porosity of porous solids," *ACTA Acustica united with Acustica,* vol. 91, no. 2, pp. 342-348, 2005.

[12] A. Cummings and S. Beadle, "Acoustic properties of reticulated plastic foams," *Journal of sound and vibration,* vol. 175, no. 1, pp. 115-133, 1994.

[13] N. Kino and T. Ueno, "Comparisons between characteristic lengths and fibre equivalent diameters in glass fibre and melamine foam materials of similar flow resistivity," *Applied Acoustics,* vol. 69, no. 4, pp. 325-331, 2008.

[14] *Acoustics – Measurement of sound absorption in a reverberation room*, ISO 354:2003(E).

[15] W. Lauriks, A. Cops, and P. Belien, "The influence of the edge effect on the statistical absorption coefficient," *Acta Acustica united with Acustica,* vol. 70, no. 2, pp. 155-159, 1990.

[16] M. Vercammen, "Improving the accuracy of sound absorption measurement according to ISO 354," in *Proceedings of the International Symposium on Room Acoustics*, 2010: Melbourne, Australia, pp. 29-31.

[17] *Acoustics — Determination of sound absorption coefficient and impedance in impedance tubes — Part 2: Transfer-function method*, ISO 10534-2(E).

[18] P. B. Murray, J. T. Kunio, L. Christensen, and F. S. Larsen, "Use of a Portable Flanged Impedance Tube for Absorber Design and Measurement," SAE Technical Paper, 0148-7191, 2015.

[19] *Acoustics — Measurement of sound absorption properties of road surfaces in situ — Part 2: Spot method for reflective surfaces*, ISO 13472-2:2010(E).

[20] P. Dickinson and P. Doak, "Measurements of the normal acoustic impedance of ground surfaces," *Journal of Sound and Vibration,* vol. 13, no. 3, pp. 309-322, 1970.

[21] E. Tijs, "Study and development of an in situ acoustic absorption measurement method," PhD Thesis, 2013.

[22] C.-H. Jeong, "Guideline for adopting the local reaction assumption for porous absorbers in terms of random incidence absorption coefficients," *Acta Acustica united with Acustica,* vol. 97, no. 5, pp. 779-790, 2011.

[23] E. Brandão, A. Lenzi, and J. Cordioli, "Estimation and minimization of errors caused by sample size effect in the measurement of the normal absorption coefficient of a locally reactive surface," *Applied Acoustics,* vol. 73, no. 6-7, pp. 543-556, 2012.

[24] M. Li, W. van Keulen, E. Tijs, M. van de Ven, and A. Molenaar, "Sound absorption measurement of road surface with in situ technology," *Applied Acoustics,* vol. 88, pp. 12-21, 2015.

[25] A. Pedrero, M. Á. Navacerrada, D. de la Prida, L. Iglesias, and A. Díaz-Chyla, "On the accuracy of the sound absorption measurement with an impedance gun," *Applied Acoustics,* vol. 158, p. 107039, 2020.

[26] F. Jacobsen and V. Jaud, "A note on the calibration of pressure-velocity sound intensity probes," *The Journal of the Acoustical Society of America,* vol. 120, no. 2, pp. 830-837, 2006.

[27] R. Lanoye, G. Vermeir, W. Lauriks, R. Kruse, and V. Mellert, "Measuring the free field acoustic impedance and absorption coefficient of sound absorbing materials with a combined particle velocity-pressure sensor," *The Journal of the Acoustical Society of America,* vol. 119, no. 5, pp. 2826-2831, 2006.

[28] P. Cats, E. Tijs, and D. F. Comesana, "Exploration of the differences between a pressure-velocity based in situ absorption measurement method and the standardized reverberant room method," in *Proceedings of Meetings on Acoustics*, 2013, vol. 19, no. 1: AIP Publishing.

[29] Y. Champoux, J. Nicolas, and J. Allard, "Measurement of acoustic impedance in a free field at low frequencies," *Journal of sound and vibration,* vol. 125, no. 2, pp. 313-323, 1988.

[30] U. Ingård and R. Bolt, "A free field method of measuring the absorption coefficient of acoustic materials," *The Journal of the Acoustical Society of America,* vol. 23, no. 5, pp. 509-516, 1951.

[31] B. B. de La Hosseraye, M. Hornikx, and J. Yang, "In situ acoustic characterization of a locally reacting porous material by means of PU measurement and model fitting," *Applied Acoustics,* vol. 191, p. 108669, 2022.

[32] Z.-W. Luo, C.-J. Zheng, Y.-B. Zhang, and C.-X. Bi, "Estimating the acoustical properties of locally reactive finite materials using the boundary element method," *The Journal of the Acoustical Society of America,* vol. 147, no. 6, pp. 3917-3931, 2020.

[33] E. Brandão, P. Mareze, A. Lenzi, and A. R. da Silva, "Impedance measurement of non-locally reactive samples and the influence of the assumption of local reaction," *The Journal of the Acoustical Society of America,* vol. 133, no. 5, pp. 2722-2731, 2013.

[34] E. Paris, "L. On the coefficient of sound-absorption measured by the reverberation method," *The London, Edinburgh, and Dublin Philosophical Magazine and Journal of Science,* vol. 5, no. 29, pp. 489-497, 1928.

[35] A. London, "The determination of reverberant sound absorption coefficients from acoustic impedance measurements," *The Journal of the Acoustical Society of America,* vol. 22, no. 2, pp. 263-269, 1950.

[36] S.-I. Thomasson, "On the absorption coefficient," *Acta Acustica united with Acustica,* vol. 44, no. 4, pp. 265-273, 1980.

[37] J. Brunskog, "The forced sound transmission of finite single leaf walls using a variational technique," *The Journal of the Acoustical Society of America,* vol. 132, no. 3, pp. 1482-1493, 2012.

[38] M. Pereira, P. Mareze, L. Godinho, P. Amado-Mendes, and J. Ramis, "Proposal of numerical models to predict the diffuse field sound absorption of finite sized porous materials–BEM and FEM approaches," *Applied Acoustics,* vol. 180, p. 108092, 2021.

[39] F. Glover, "A template for scatter search and path relinking," in *European conference on artificial evolution*, 1997: Springer, pp. 1-51.

[40] S. Thomasson, "Theory and experiments on the sound absorption as a function of area, report TRITA_TAJ 8201," *Royal Institute of Technology, Stockholm,* 1982.

[41] I. BIPM, I. IFCC, I. ISO, and O. IUPAP, "Evaluation of measurement data—guide to the expression of uncertainty in measurement, JCGM 100: 2008 GUM 1995 with minor corrections," *Joint Committee for Guides in Metrology,* vol. 98, 2008.

APPENDICES

A - 1 PU Probe measurements on 1230x1230mm² sample of melamine foam of 50mm thickness

	Melamine 1230x1230mm²											
	Center						Confidence					
	PWA			MS			PWA			MS		
Freq (Hz)	Measured	Rel. error	Abs. Error	Measured	Rel. error	Abs. Error	Measured	Rel. error	Abs. Error	Measured	Rel. error	Abs. Error
315	-0.0419	115%	0.328	-0.0100	104%	0.296	0.0425	85%	0.243	-0.1527	153%	0.438
400	0.3110	22%	0.085	0.3028	24%	0.094	0.5205	31%	0.124	0.4815	21%	0.085
500	0.4140	21%	0.110	0.4571	13%	0.067	0.4556	13%	0.068	0.4156	21%	0.109
630	0.6370	3%	0.020	0.6343	3%	0.023	0.5637	14%	0.094	0.5352	19%	0.122
800	0.7920	1%	0.011	0.7795	0%	0.001	0.8303	6%	0.050	0.8230	5%	0.042
1000	0.9020	2%	0.019	0.8982	2%	0.015	0.9098	3%	0.027	0.9032	2%	0.020
1250	0.9760	2%	0.021	0.9750	2%	0.020	0.9836	3%	0.029	0.9821	3%	0.027
1600	0.9990	1%	0.007	0.9994	1%	0.008	0.9982	1%	0.006	0.9981	1%	0.006
2000	0.9880	1%	0.005	0.9878	1%	0.005	0.9804	1%	0.013	0.9787	1%	0.014
2500	0.9720	0%	0.004	0.9719	0%	0.004	0.9610	1%	0.007	0.9579	1%	0.010
3150	0.9510	0%	0.000	0.9503	0%	0.000	0.9578	1%	0.007	0.9545	0%	0.004
4000	0.9730	0%	0.003	0.9730	0%	0.003	0.9873	1%	0.012	0.9863	1%	0.010
5000	1.0000	1%	0.007	0.9999	1%	0.007	0.9992	1%	0.006	0.9991	1%	0.006
6300	0.9860	1%	0.006	0.9860	1%	0.006	0.9878	1%	0.008	0.9869	1%	0.007
8000	0.9980	0%	0.003	0.9976	0%	0.003	0.9967	0%	0.002	0.9965	0%	0.001
10000	0.9940	0%	0.001	0.9950	0%	0.002	0.9957	0%	0.003	0.9954	0%	0.002
400-800Hz		12%			10%			16%			17%	
800-10000Hz		1%			1%			2%			1%	

A - 2 PU Probe measurements on 200x200mm² sample of melamine foam of 50mm thickness

	Melamine 200x200mm²											
	Center						Confidence					
	PWA			MS			PWA			MS		
Freq (Hz)	Measured	Rel. error	Abs. Error	Measured	Rel. error	Abs. Error	Measured	Rel. error	Abs. Error	Measured	Rel. error	Abs. Error
315	0.0300	89%	0.2557	0.1066	63%	0.1791	0.1140	60%	0.1717	0.0381	87%	0.2476
400	0.3435	13%	0.0528	0.3904	1%	0.0059	0.3936	1%	0.0027	0.3472	12%	0.0491
500	0.3941	25%	0.1300	0.4370	17%	0.0871	0.4060	23%	0.1181	0.3589	32%	0.1652
630	0.5167	21%	0.1405	0.5496	16%	0.1076	0.5184	21%	0.1388	0.4831	26%	0.1741
800	0.7318	6%	0.0490	0.7446	5%	0.0362	0.6855	12%	0.0953	0.6683	14%	0.1126
1000	0.9151	4%	0.0323	0.9206	4%	0.0378	0.9004	2%	0.0176	0.8937	1%	0.0109
1250	0.9963	4%	0.0415	0.9967	4%	0.0419	0.9962	4%	0.0414	0.9957	4%	0.0409
1600	0.9865	1%	0.0053	0.9874	0%	0.0044	0.9883	0%	0.0035	0.9874	0%	0.0045
2000	0.9675	3%	0.0256	0.9700	2%	0.0231	0.9574	4%	0.0357	0.9539	4%	0.0392
2500	0.9782	1%	0.0101	0.9799	1%	0.0118	0.9459	2%	0.0222	0.9417	3%	0.0264
3150	0.9573	1%	0.0066	0.9605	1%	0.0098	0.9471	0%	0.0036	0.9428	1%	0.0079
4000	0.9740	0%	0.0019	0.9759	0%	0.0001	0.9793	0%	0.0034	0.9776	0%	0.0018
5000	0.9988	1%	0.0055	0.9989	1%	0.0056	0.9962	0%	0.0029	0.9959	0%	0.0026
6300	0.9834	0%	0.0031	0.9846	0%	0.0043	0.9829	0%	0.0026	0.9816	0%	0.0013
8000	0.9961	0%	0.0010	0.9962	0%	0.0012	0.9935	0%	0.0015	0.9930	0%	0.0020
10000	0.9944	0%	0.0015	0.9949	0%	0.0020	0.9935	0%	0.0006	0.9929	0%	0.0000
400-800Hz		16%			10%			14%			21%	
800-10000Hz		2%			2%			2%			2%	

A - 3 PU Probe measurements on 1350x1200mm² sample of rockwool PN70 of 50mm thickness

	Rockwool 1350x1200mm²											
	Center						Confidence					
	PWA			MS			PWA			MS		
Freq (Hz)	Measured	Rel. error	Abs. Error	Measured	Rel. error	Abs. Error	Measured	Rel. error	Abs. Error	Measured	Rel. error	Abs. Error
315	0.1758	59%	0.2529	0.1714	60%	0.2574	0.2981	30%	0.1306	0.2354	45%	0.1933
400	0.4291	22%	0.1197	0.4560	17%	0.0928	0.4866	11%	0.0622	0.4484	18%	0.1004
500	0.5667	15%	0.1009	0.5524	17%	0.1153	0.5577	16%	0.1099	0.5402	19%	0.1274
630	0.6628	14%	0.1082	0.6974	10%	0.0736	0.7102	8%	0.0607	0.6912	10%	0.0798
800	0.7654	10%	0.0820	0.7991	6%	0.0483	0.7769	8%	0.0705	0.7649	10%	0.0825
1000	0.8469	5%	0.0461	0.8688	3%	0.0242	0.8543	4%	0.0387	0.8315	7%	0.0615
1250	0.8824	3%	0.0284	0.9161	1%	0.0053	0.8924	2%	0.0184	0.8845	3%	0.0263
1600	0.9046	1%	0.0056	0.9275	2%	0.0173	0.9048	1%	0.0054	0.9010	1%	0.0093
2000	0.8978	1%	0.0088	0.9125	1%	0.0060	0.9052	0%	0.0014	0.8965	1%	0.0100
2500	0.9252	1%	0.0084	0.9339	2%	0.0171	0.9316	2%	0.0148	0.9270	1%	0.0102
3150	0.9396	0%	0.0042	0.9384	1%	0.0054	0.9424	0%	0.0014	0.9377	1%	0.0061
4000	0.9655	0%	0.0016	0.9635	0%	0.0005	0.9686	0%	0.0047	0.9662	0%	0.0022
5000	0.9719	1%	0.0053	0.9717	1%	0.0051	0.9731	1%	0.0065	0.9710	0%	0.0043
6300	0.9774	0%	0.0022	0.9779	0%	0.0027	0.9799	0%	0.0047	0.9783	0%	0.0031
8000	0.9819	0%	0.0009	0.9836	0%	0.0026	0.9850	0%	0.0040	0.9838	0%	0.0028
10000	0.9878	0%	0.0021	0.9894	0%	0.0037	0.9909	1%	0.0052	0.9902	0%	0.0045
400-800Hz		15%			12%			11%			14%	
800-10000Hz		2%			1%			2%			2%	

A - 4 PU Probe measurements on 200x200mm² sample of rockwool PN70 of 50mm thickness

	Rockwool 200x200mm²											
	Center						Confidence					
	PWA			MS			PWA			MS		
Freq (Hz)	Measured	Rel. error	Abs. Error	Measured	Rel. error	Abs. Error	Measured	Rel. error	Abs. Error	Measured	Rel. error	Abs. Error
315	-0.0361	108%	0.4649	0.0502	88%	0.3785	0.0566	87%	0.3722	-0.0329	108%	0.4616
400	0.3698	33%	0.1790	0.4149	24%	0.1339	0.3290	40%	0.2197	0.2755	50%	0.2733
500	0.3623	46%	0.3054	0.3737	44%	0.2940	0.2217	67%	0.4459	0.2121	68%	0.4556
630	0.6945	10%	0.0765	0.7144	7%	0.0565	0.5791	25%	0.1919	0.5492	29%	0.2217
800	0.8634	2%	0.0161	0.8711	3%	0.0237	0.7520	11%	0.0954	0.7382	13%	0.1092
1000	0.9020	1%	0.0090	0.9142	2%	0.0212	0.8834	1%	0.0096	0.8696	3%	0.0234
1250	0.8687	5%	0.0421	0.8772	4%	0.0336	0.9452	4%	0.0344	0.9407	3%	0.0299
1600	0.8219	10%	0.0883	0.8297	9%	0.0805	0.9433	4%	0.0331	0.9408	3%	0.0306
2000	0.7800	14%	0.1265	0.8137	10%	0.0928	0.8987	1%	0.0078	0.8894	2%	0.0172
2500	0.9651	5%	0.0483	0.9673	6%	0.0504	0.9118	1%	0.0050	0.9065	1%	0.0104
3150	0.9402	0%	0.0036	0.9446	0%	0.0008	0.9053	4%	0.0386	0.8977	5%	0.0461
4000	0.9656	0%	0.0017	0.9681	0%	0.0042	0.9720	1%	0.0080	0.9698	1%	0.0058
5000	0.9745	1%	0.0079	0.9764	1%	0.0098	0.9655	0%	0.0011	0.9628	0%	0.0038
6300	0.9824	1%	0.0072	0.9837	1%	0.0085	0.9730	0%	0.0022	0.9708	0%	0.0043
8000	0.9863	1%	0.0053	0.9873	1%	0.0063	0.9782	0%	0.0028	0.9765	0%	0.0045
10000	0.9915	1%	0.0059	0.9922	1%	0.0065	0.9875	0%	0.0018	0.9865	0%	0.0008
400-800Hz		23%			20%			36%			40%	
800-10000Hz		3%			3%			2%			3%	

A - 5 PU probe in situ measurement guidelines

Based on the findings from prior research studies and the outcomes of the sensitivity analysis conducted using 50mm thick melamine foam and rockwool samples, the following guidelines are recommended to be followed when performing in-situ measurements with the Impedance Gun measurement system. The ensuing set of guidelines is bifurcated into two categories, delineating the employment (or non-employment) of an inverse methodology solution.

Basic guidelines for sound absorption characterization of porous materials with a PU Probe:

- Sample sizes should be as large as possible to avoid edge effects.
- Measurements using the Mirror Source model are preferred over the Plane Wave model.
- The PU Probe should be located as far from the edges as possible, and vertically within 20mm from the sample surface.
- Highly reflective materials should be avoided. Thicker, more absorptive materials will yield best results.
- Measurements should only be performed at normal incidence.
- Values below 800 Hz are prone to high uncertainties, leading to an underestimation of the absorption coefficient.

In case of employment of a model fitting postprocessing solution:

- Sample sizes can be kept as small as 200x200mm^2.
- In case of unknown material thickness, this parameter should be set as a variable in the code, inputting an estimate thickness value.
- The frequency range of the model fitting should be set to 800-10000Hz, for porous samples sizes down to 200x200mm^2.
- Retrieved non-acoustic parameters should be considered as an estimate and the validity range should be carefully checked. Direct measurements are still preferred.